MEMORANDUM REPORT ARBRL-MR-03281

AERODYNAMICS OF ASYMMETRIC SABOT DISCARD

Edward M. Schmidt
Peter Plostins

June 1983

US ARMY ARMAMENT RESEARCH AND DEVELOPMENT COMMAND
BALLISTIC RESEARCH LABORATORY
ABERDEEN PROVING GROUND, MARYLAND

Destroy this report when it is no longer needed.
Do not return it to the originator.

Additional copies of this report may be obtained from the National Technical Information Service, U. S. Department of Commerce, Springfield, Virginia 22161.

The findings in this report are not to be construed as an official Department of the Army position, unless so designated by other authorized documents.

The use of trade names or manufacturers' names in this report does not constitute indorsement of any commercial product.

UNCLASSIFIED

SECURITY CLASSIFICATION OF THIS PAGE *(When Data Entered)*

REPORT DOCUMENTATION PAGE		READ INSTRUCTIONS BEFORE COMPLETING FORM
1. REPORT NUMBER MEMORANDUM REPORT ARBRL-MR-03281	2. GOVT ACCESSION NO.	3. RECIPIENT'S CATALOG NUMBER
4. TITLE *(and Subtitle)* AERODYNAMICS OF ASYMMETRIC SABOT DISCARD		5. TYPE OF REPORT & PERIOD COVERED Final 6. PERFORMING ORG. REPORT NUMBER
7. AUTHOR(s) Edward M. Schmidt and Peter Plostins		8. CONTRACT OR GRANT NUMBER(s)
9. PERFORMING ORGANIZATION NAME AND ADDRESS US Army Ballistic Research Laboratory ATTN: DRDAR-BLL Aberdeen Proving Ground, MD 21005		10. PROGRAM ELEMENT, PROJECT, TASK AREA & WORK UNIT NUMBERS RDT&E 1L162618AH80
11. CONTROLLING OFFICE NAME AND ADDRESS US Army Armament Research & Development Command US Army Ballistic Research Laboratory (DRDAR-BLA-S) Aberdeen Proving Ground, MD 21005		12. REPORT DATE June 1983 13. NUMBER OF PAGES 52
14. MONITORING AGENCY NAME & ADDRESS*(if different from Controlling Office)*		15. SECURITY CLASS. *(of this report)* Unclassified 15a. DECLASSIFICATION/DOWNGRADING SCHEDULE

16. DISTRIBUTION STATEMENT *(of this Report)*

Approved for public release; distribution unlimited.

17. DISTRIBUTION STATEMENT *(of the abstract entered in Block 20, if different from Report)*

18. SUPPLEMENTARY NOTES

19. KEY WORDS *(Continue on reverse side if necessary and identify by block number)*

Sabot Discard
Aerodynamic Interference
Asymmetric Flow
Launch Disturbances

20. ABSTRACT *(Continue on reverse side if necessary and identify by block number)* EMS/PP/NER

Experimental results are presented which examine the pressure distributions upon projectiles during the portion of the launch cycle which involves strong aerodynamic interference between the flight body and sabot components. Particular attention is given to the simulation of asymmetric sabot discard geometries since these configurations result in transverse loadings upon the projectile. The pressure distribution in a given section of the projectile surface is shown to be strongly influenced only by the flow field associated with the sabot component

DD FORM 1 JAN 73 1473 EDITION OF 1 NOV 65 IS OBSOLETE

UNCLASSIFIED

SECURITY CLASSIFICATION OF THIS PAGE *(When Data Entered)*

facing that section. The basic features of the flow are similar in both the symmetric and asymmetric cases. The experiment is compared with existing analytical models and recommendations for improvements are made.

TABLE OF CONTENTS

LIST OF ILLUSTRATIONS

LIST OF ILLUSTRATIONS

I. INTRODUCTION

Sabots are employed to reduce the sectional density of projectiles permitting the attainment of high in-bore accelerations. Once free of the gun, the sabots must be discarded in order to decrease the drag of the round. It has been demonstrated [1-4] that aerodynamic interference during this process can adversely affect the projectile trajectory and increase on-target dispersion. While the flow field associated with symmetric sabot discard geometries has been investigated [5-8], there is no body of information describing the asymmetric case. The report discusses the results of an experimental program to obtain preliminary data on asymmetric discard.

Both spin and fin stabilized projectiles are launched with the aid of sabots. Currently, finners are of interest since they represent the most practical means of stabilizing the long rod penetrators which have demonstrated effectiveness against armor. In order to be fielded, a design must achieve a high degree of precision implying the need to minimize round-to-round dispersion. In-bore dynamics dominate the launch process. The lateral motions of the gun tube and of sabot/projectile relative to the gun tube provide the initial dynamics to the exiting round. Of the post

---

1. *H. Conn, "The Influence of Sabot Separation on the Yawing Motion of a Cone," Defense Research Establishment, Valcartier,* Canada, *TN 1849/70, June 1970.*

2. *W. D. Glauz, "Estimation of Forces on a Flechette Resulting from a Shock Wave," Midwest Research Institute, Kansas City, MO, R3451-E, May 1971.*

3. *E. M. Schmidt and D. D. Shear, "Aerodynamic Interference During Sabot Discard," AIAA JSR, Vol. 15, No. 3, May-June 1978, pp 162-167.*

4. *E. M. Schmidt, "Disturbances to the Launch of Fin-Stabilized Projectiles,"AIAA JSR, Vol. 19, No. 1, January-February 1982, pp 30-35.*

5. *D. Siegelman and P. Crimi, "Projectile/Sabot Discard Aerodynamics," BRL Contract Report 00410, Ballistic Research Laboratory, APG, MD, December 1979 (AD 080538).*

6. *D. Siegelman, P. Crimi, and E. M. Schmidt, "Projectile/Sabot Discard Aerodynamics," AIAA Paper No. 80-1588, August 1980.*

7. *D. Siegelman, J. Wang, and E. M. Schmidt, "Sabot Design Optimization," AIAA JSR, Vol. 19, No. 3, May-June 1982, pp 197-198.*

8. *E. M. Schmidt, "Wind-Tunnel Measurements of Sabot-Discard Aerodynamics," AIAA JSR, Vol. 18, No. 3, May-June 1981, pp 235-240.*

separation disturbances, aerodynamic interference during sabot discard has been shown to be most significant [4]. The controlling asymmetries may be grouped into two broad categories: first, cases where the projectile yaws with respect to the sabot components and, second, cases where the sabot discard geometry is asymmetric with respect to the projectile. Either favorable or unfavorable interference may be observed. For example, a projectile launched with a high initial yaw rate may have this rate damped during the discard process. Alternatively, asymmetries in the sabot discard have been shown to induce significant projectile yaw rates.

A typical fin-stabilized projectile and its associated sabots are shown in Figure (1). Generally, the sabot is segmented into either three or four components. As these separate, the flow about the projectile undergoes dramatic changes as illustrated in Figures 2a-2d. This sequence of spark shadowgraphs covers the conditions from penetration of the muzzle blast through entry into unconstrained free flight. Near the muzzle (Figure 2a), the strong confinement provided by the tightly grouped sabot components causes the boundary layer on the projectile to separate at the conical tip. Glotz [9] has conducted wind tunnel tests showing that the shock structure on the tip is not necessarily stable during this period and that flow oscillations, similar to those observed on spike nosed bodies, are possible. As the components open, the separation bubble on the nose collapses (Figure 2b); however, intersection of the sabot shocks with the projectile results in separation on the cylindrical section. A relatively strong shock is associated with this separated flow. Additionally, asymmetry in the separation is noticed in comparing the upper and lower surfaces. Further lateral motion of the sabot components weakens the strength of the shocks impinging upon the projectile (Figure 2c). In this case, while boundary layer separation is evident, the associated compression is rather weak. Finally, the components move away from the projectile and interactions cease (Figure 2d).

Glauz [2] considers the interference between a single sabot component and a fin-stabilized projectile. He notes that the impingement and reflection of the sabot shock wave off the projectile is complicated even if only inviscid flow is considered (Figure 3). The intersection of the shock and the cylindrical section of the projectile is curved. On the upper surface, the shock deflects the flow directly onto the body; while, on the 90-degree lateral surface of the cylinder, a glancing intersection occurs. Thus, the shock would reflect from the upper surface (either a regular or Mach stem reflection is possible depending upon local Mach number and incidence angle) but pass the lateral surface relatively intact. On the underside, the shock would tend to deflect the flow away from the surface, which could result in cross flow separation. It would be expected that the pressure distribution would have a maximum on the upper surface and decay around the perimeter.

---

9. *G. Glotz, "Investigation of the Stability of Flow during the Sabot Discard Process," Proceedings of the 6th International Symposium on Ballistics, American Defense Preparedness Association, Arlington, VA, October 1981.*

Glauz notes that the presence of viscous effects results in the possibility of three dimensional, shock-boundary layer interactions where separated flow and strong cross flows could influence the pressure distribution on the body. While noting the presence of these factors, Glauz analyzes the interaction by assuming that the sabot shock is a simple, planar oblique shock and treats the projectile using potential flow theory. His results show that the fins dominate as a source of lateral loads.

Siegelman and Crimi [5,6] develop an approximate model of the flow about the projectile and symmetrically discarding sabot components. The analysis is based upon wind tunnel measurements of the pressure distributions on these bodies [8]. The sabot is approximated as an axially symmetric body (sphere-cylinder). The flow field is computed with a blunt body code [10] and used to determine the intersection of the sabot shock with the projectile surface. The pressure level on the surface is determined by assuming a locally two-dimensional inviscid reflection process. Viscous effects are included using correlations based upon measured interactions between shock waves and turbulent boundary layers. No variation in pressure in the azimuthal direction is addressed. Siegelman, et al [7] use this model of interference aerodynamics to define an interaction parameter which quantifies the magnitude of sabot discard perturbation.

In order to better define these disturbances, data are required which examine the actual flow associated with asymmetric discard. This report presents the results of a study of the flow associated with two categories of asymmetric discard: a single sabot component moving laterally away from a projectile, and three sabot components, one of which is moved with respect to the remaining stationary components. The data are used to examine the zones of influence of sabot flowfields, the validity of approximate models, and to suggest possible improvements to these models. Additionally, a sabot discard strategy to minimize aerodynamic interference is suggested and tested in range firings.

II. MODEL DESIGN AND TEST PROCEDURE

The pressure distributions on models of a projectile and sabot component were measured in the Hypersonic Leg of the NASA Langley Unitary Plan Facility. The projectile was mounted on a sting extending from a window blank, while the sabot was mounted on the main trapeze of the wind tunnel. Three configurations were tested: the projectile and a single sabot component; the projectile and three sabot components, one of which is moved relative to the others (Figure 4a); and the projectile with one component and a 120-degree splitter plate (Figure 4b). The latter data represent the baseline, symmetric

---

10. G. Moretti and M. Abbett, "A Time-Dependent Computational Method for Blunt Body Flows," AIAA J, Vol. 4, No. 12, December 1966, pp 2136-2141.

discard configuration and have been previously reported [8].

The projectile (Figure 5) is a stainless steel cone cylinder having a diameter of 50.8mm, a length-to-diameter ratio of 10.5, and a 30-degree total included angle conical nose. Fins were not installed on the models tested. Fifty static pressure orifices are positioned on the surface between the 120-degree planes of symmetry. The sabot is brass and has cylindrical inner and outer surfaces of radii 25.4 and 76.2mm, respectively. The leading edge of the sabot has a 40-degree chamfer. Fifty pressure orifices are located on the surfaces facing the projectile. Pressures were measured by Scani-valve transducers external to the tunnel.

The splitter plates are fabricated from 6.35mm thick stainless steel plates having dimensions of 0.41m x 0.44m. The leading edges are chamfered at a 15-degree angle. No pressure orifices are located on the plates. The plates are intended to provide reflecting surfaces at natural symmetry planes in the flow field. In this manner, the requirement to actuate three sabot components simultaneously is avoided, and the symmetric discard geometry is easily duplicated. Unfortunately, the boundary layers on these plates and at the projectile-plate corners cause degradation of the data due to shock-boundary layer interactions [8].

The static sabot components (Figure 4a) are fabricated from brass to the identical geometry of the actuated component; however, no instrumentation is included. The two static sabot components are mounted at zero angle of attack and at a separation distance of 3.81cm from the surface of the projectile. This configuration was designed to provide a validation of the splitter plate technique at a predetermined geometry [8]. The geometry was selected since preliminary computations indicated that the area between sabot components was sufficient to pass the entry mass flow. In the present study, the configuration provides a source to test the influence of discard asymmetry where one sabot component is free to move relative to the others.

The size of the 4x4 foot test section permitted the sabot component to be moved relative to the projectile over an angular range of 0-18 degrees in pitch and laterally from 3.2 to 114 mm. This range simulated a significant portion of the region of interest. Tests were conducted at a Mach number of 4.5, which is representative of flight Mach numbers. A comparison of flight and test conditions is given in Table 1. Due to wind tunnel operation limits, the flight conditions could not be duplicated in the tests. The heat transfer characteristics were not of interest in this experiment; therefore, simulation of stagnation temperature is not a serious drawback. However, as previously noted [8] viscous interactions are observed in the experimental results, and a closer duplication in Reynolds Number would have been worthwhile.

TABLE 1. FLIGHT AND TEST CONDITIONS

PARAMETER	WIND TUNNEL	FREE FLIGHT
M	4.5	4.5
RE (1/M)	6.6×10^6	$89.\times10^6$
T (DEG.K)	353.	1487.
P (N/M)	2.45×10^5	2.93×10^7

The data describing pressure distribution on the sabot component are not considered here. Only the pressure distribution on the projectile will be considered in detail. Various configurations are examined to define the interactions between the sabot component flow fields and the projectile. The data acquired with the splitter plates define the basic flow field for symmetric discard. The results with the single sabot component provide information on one category of asymmetric interaction and, when compared with the splitter plate data, give an indication of the extent of mutual reinforcement between adjacent components. Finally, the measurements taken with three sabot components in place are used to examine both symmetric and asymmetric properties.

III. TEST RESULTS

The features of the projectile surface pressure distribution during the interaction phase of sabot discard are shown in Figure 6. The three sabot configurations, i.e., single sabot, three sabots, and the sabot with splitter plates on the projectile, are compared for the geometry designed as a symmetry check case. The three pressure profiles are taken along the plane of symmetry and clearly show the arrival and reflection of the sabot shock wave. The pressure peaks occur within a body radius for each case. (It should be noted that due to the interval between pressure orifices, the peaks could not be located exactly.) The peak values are similar for the single and triple sabot cases and slightly lower with the splitter plates. The pressure level ahead of the shock intersection becomes progressively greater as the effective obstruction to the flow increases. For the single sabot component, the pressure ahead of the intersection approaches the undisturbed level; i.e., the pressure ratio equals one. With three components in place, mutual reinforcement of the impinging shocks apparently separates the boundary layer completely around the periphery of the body resulting in a characteristic

pressure plateau. With splitter plates, this interaction is even more pronounced. Downstream of the intersection, the pressures rapidly decay as the corner expansion from the sabot arrives at the surface.

The influence of mutual reinforcement from adjacent sabot components is illustrated by Figure 7. This plot presents the variation in projectile centerline pressure with forward displacement of the free sabot in the three sabot arrangement. The static sabot components remain at a fixed axial location relative to the projectile. It is noted that the pressure pulse moves forward with the component and only relatively minor changes are observed. This indicates that, as expected, the incident shock from the facing sabot component dominates the surface pressure distribution on the projectile. The glancing shocks from adjacent components do not significantly influence or reinforce the primary interaction.

Further emphasis of this point is obtained by comparing the azimuthal pressure distributions for the geometry of the symmetry check case (Figures 8a-8c). For azimuthal angle of 0, 30, and 45 degrees, the pressure distributions for the single and triple sabot component cases are essentially identical. The most significant difference is observed in the region of the pressure plateau forward of the shock intersection. It is noteworthy that the level of the pressure in this region is roughly constant both in the axial and azimuthal directions. As the azimuth angle increases, the peak pressure decreases significantly reflecting the change in the local flow deflection angle around the periphery of the cylinder. Again, the similarity between the pressure profiles for the single asymmetric sabot case and the symmetric, triple configuration is taken to indicate that mutual reinforcement by adjacent sabot components is not significant.

During discard, the sabot components pitch to positive angles of attack and move laterally away from the projectile. Pressure distributions representative of the trends due to this motion are presented for the sabot displacing laterally while at zero and ten degree angles of attack in Figures 9 and 10, respectively. Included in the figures are profiles for the single sabot and splitter plate cases. As the sabot moves away from the projectile, the peak pressure decays and the location of the peak displaces aft. This behavior is obviously expected as the source of disturbance becomes more distant. The results with the splitter plates and the single sabot component are in good qualitative agreement and at the more distant separations overlap. The effect of angle of attack is to displace the leading edge of the sabot away from the projectile surface, bringing about decreased peak pressure and aft motion of the shock impingement.

The variation in location and magnitude of the peak pressure with sabot motion is summarized for the two test arrangements in Figures 11a and 11b. The predictions of the approximate model of Siegelman and Crimi [5] are included. The model predicts the correct trends in both the impingement location and pressure level as the sabot position changes; however, quantitative agreement is lacking and certain features of the model are not observed in the experiment. In particular, the transition from Mach to regular reflection as indicated by the discontinuities in the predicted pressure variations is not seen. To improve the prediction, a different

treatment of the sabot and projectile flow fields is attempted.

IV. FLOW FIELD MODEL

The primary characteristic of the experimental projectile pressure distributions is the large pressure pulse due to impingement of the sabot component bow shock (Figure 6). Immediately following the pressure rise is a sudden drop-off in pressure. This pressure decay is caused by the expansion generated at the sabot component corner reaching the projectile surface. As an example consider a generic 2-D sabot component with a wedge angle of 38 degrees flying at zero angle of attack at Mach 4.5. The wave pattern generated by a 2-D shock expansion is given in Figure 12a. The pressure distribution on a plane wall four calibers from the sabot component is given in Figure12b. Clearly the shape of the pressure distribution obtained is identical to those exhibited by the experimental data. The fact that the actual flow field is 3-D and highly interactive only alters the pulse peak pressure level. Naturally, viscosity tends to spread the pulse width.

The above example provides an explanation of the shape of the pressure distribution on the projectile; however, an attempt will now be made at a more realistic solution. Consider a single 2-D sabot component at an angle of attack flying next to an axisymmetric projectile. The projection in the plane bisecting both the sabot component and the projectile is shown in Figure 5. In order to predict the sabot bow shock-projectile shock interaction and the resulting projectile pressure distribution, approximate shock shapes for both bodies are needed. The projectile shock shape is generated by solving for the projectile flow field by the method of characteristics. The sabot behaves like a blunt body so a shock layer approach which solves the integral form of the continuity equation for the stand-off distance is used. The intersection point of the sabot bow shock and the projectile shock is thus determined and a locally 2-D shock expansion is utilized to compute the impact location of the sabot bow shock on the projectile surface.

The following method generates the sabot shock shape. In the coordinate system given in Figure 13 the mass entering the shock layer from the freestream is given by:

$$\dot{m} = \rho_\infty V_\infty h \tag{1a}$$

$$h = x \sin(40^\circ+\alpha)+\Delta\sin(\phi-\alpha) \tag{1b}$$

$$h=x_{ff}\sin(40^\circ+\alpha)+(x-x_{ff})\sin(\alpha)+\Delta\sin(\phi-\alpha) \tag{1c}$$

The mass leaving the layer at any given "x" station is:

$$\dot{m} = \rho_s u_s \Delta \int_0^{1.0} \hat{\rho}\, \hat{u}\, d\beta \tag{2a}$$

$$\beta = \frac{y}{\Delta} \qquad \hat{\rho} = \rho/\rho_s \qquad \hat{u} = u/u_s \tag{2b}$$

Equating Equations (1a) and (2a) results in:

$$\Delta = h/\overline{\rho}_s \overline{u}_s \int_0^{1.0} \hat{\rho}\, \hat{u}\, d\beta \tag{3}$$

In order to obtain a value of the standoff distance at any "x" location an a priori knowledge of the density and velocity profiles is assumed. For a first approximation, a constant density shock layer is assumed:

$$\hat{\rho} = 1.0 \tag{4}$$

The velocity profile $\hat{u} = \hat{u}(x,y)$ presents somewhat more of a problem.

In the stagnation region, a shock layer solution [11] shows that the velocity profile was linear in the inviscid limit and varies as shown in Figure 14a. On the front face of the sabot component, similarity is assumed and the profile of Figure 14a is used; however, to account for the expansion at the corner and downstream of the corner, the profile is allowed to expand to the shape given in Figure 14b. This expansion of the profile is terminated 2.5 calibers downstream of the corner because pressure data [8] on a free flying sabot component equilibrates to a constant surface value at that point. Subsequently, the profile shape is held constant.

Equation (3) may now be solved at each "x" location for a stand-off distance. To insure a unique solution, the entire flow field is globally iterated upon until Mach number one is achieved at the sabot corner. A sabot component and the computed shock shape are shown in Figure 15a for $\alpha = 18°$ and Mach number 4.5.

---

11. *P. Plostins and S. G. Rubin, "The Axisymmetric Stagnation Region Full Shock Layer for Large Rates of Injection," Journal of Numerical Heat Transfer, Vol. 4, 1981, pp 358-375.*

The projectile is a 15-degree cone-cylinder. Conical flow exists on the forebody up to the cone-cylinder junction. The conical solution [12] is used to initiate an axisymmetric method of characteristics solution which determines the flow field on the cylinder and the shock shape. It is a standard technique. No further explanation is needed except to say entropy effects were not included since only the shock shape and the projectile surface pressure distribution were of interest. The projectile free flight shock shape and surface pressure distribution are given in Figures 15b and 15c.

The two generated shock shapes are now used to locate the intersection point at which the sabot bow shock meets the projectile shock. At the intersection point, the strengths of the two shocks are known and a locally 2-D shock expansion procedure is used to propagate the sabot shock through the projectile flow field to the wall of the projectile, establishing the shock impact location and the over-pressure ratio. An example of the computed wave pattern and the projectile pressure distribution is given in Figure 16 for a two caliber separation, a sabot angle of attack of 18 degrees and a Mach number of 4.5. A comparision of calculated impact locations and peak overpressures to data are given in Figure 17a and 17b for various sabot separations.

The curves obtained follow the trend of the data correctly both for impact location and overpressure ratio. The absolute value of either parameter is inaccurately predicted. Several reasons for this discrepancy can be cited. One, the sabot component is 3-D and a 2-D analysis is used to predict the shock shape. Geometrically parts of the sabot component are closer to the projectile than the 2-D projection. This would tend to move the computed shock impact location forward on the projectile. Secondly, a 3-D shock is generally weaker than its 2-D counterpart and should therefore reduce the predicted overpressure levels. To improve the treatment, a 3-D shock fitting technique is under development.

V. DISCARD STRATEGY

Typical sabot designs employ leading edge chamfer or scoops to provide aerodynamic loadings which implement discard. The sabot motion combines both pitch and lateral displacement of the center of gravity relative to the projectile. A simplistic grouping of discard motion is possible (Figure 18). The first category is essentially drag dominated in that the sabot pitches to high angle of attack and, as the drag force increases, moves aft relative to the projectile. While such a process is not necessarily bad, it can create strong aerodynamic interactions between the sabot and projectile if reasonable lateral separation is not achieved. As the sabot pitches to high angle of attack, it assumes the configuration of a large, blunt body with associated strong shocks.

---

12. *J. Sims, "Supersonic Flow Around Right Circular Cones," Army Ballistic Missile Agency, Redstone Arsenal, AL, DA-TR-11-60, Mar 1960.*

The other discard group can be described as lift dominated (Figure 18b). In this case, the sabot pitches to a moderate angle of attack where it stabilizes in pitch and moves laterally away from the projectile under the action of the lift force. There are two advantages to this process. First, the sweepback angle of hypersonic shock waves is large; therefore, a given vertical displacement of the sabot results in a larger aft movement of the shock impingement point on the projectile. Second, at a moderate angle of attack, the advantages of sabot pitch in decreasing shock strength (Figure 11) are optimized.

A sample calculation of the duration of shock impingement on the projectile demonstrates these points. Postulating two sabot components starting from identical locations at zero velocity relative to the projectile and assuming that the shock is swept aft at the Mach angle in each case for the complete discard process, the interaction times are calculated to be 1.4 ms for the drag dominated case and 0.9 ms for the lift dominated case. The decreased interaction time coupled to lower pressure levels would seem to promote lifting type discard as a desirable design goal.

A firing program was conducted with two similar sabot designs; however, fins on the aft of the one sabot design provide trim stabilization and thereby implement a lifting discard. The discard trajectories were observed using orthogonal flash radiographs (Figure 19). As is observed, the standard sabot design follows a typical drag dominated discard. On the other hand, the inclusion of fins modifies this behavior providing lifting discard. While the tests demonstrated that sabot component trajectories can be controlled, subsequent firings were not convincing regarding the anticipated improvement in accuracy. Essentially no change was observed. This was primarily due to the alteration of in-bore behavior due to the stiffening of the aft of the sabot segment by the fins. As a result, the ability of the rear ramp to clamp about projectile and seal against propellant gases was degraded. The finned sabots were observed to exhibit signs of gas blow-by which were not present in the standard design.

VI. SUMMARY AND CONCLUSIONS

Results of wind tunnel tests to examine the interference aerodynamics between asymmetrically discarding sabot components and the flight body are presented. The basic features of the flow field are similar to those previously observed in tests of symmetric discard. The test results indicate that the projectile surface pressure distribution is dominated by the facing sabot component. Adjacent components do not provide significant reinforcement of the impinging shock waves. While adjacent components do influence the separated flow ahead of the shock impingement, the resulting pressure distribution is largely uniform in the axial and azimuthal direction. Thus, no significant side forces are developed. These results indicate that the asymmetric sabot discard problem can be approximated by solving for the flow field associated with one sabot component. This solution may then be applied locally to determine the interaction with the facing section of the projectile surface, thus avoiding a complex multibody solution.

Comparison with two-dimensional models of the interaction process shows that while trends in the data are qualitatively reproduced, there is disagreement between measured and predicted surface pressure distributions. To improve the prediction of the interactions, a 3-D model of the sabot component flow field is being developed.

The experiment treats only a 120-degree segment of the flow. No fin interactions are considered. Additionally, the tests were conducted at a Reynolds Number significantly below flight values. To obtain a more complete description of the flow, additional wind tunnel tests are planned.

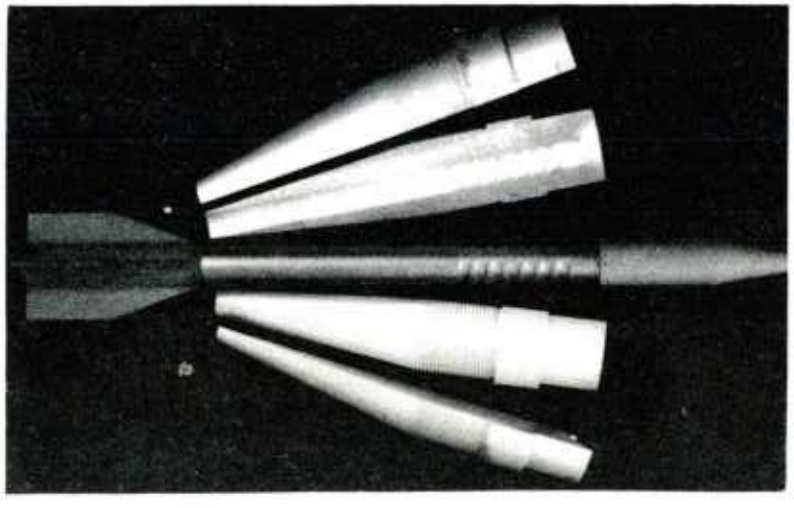

Figure 1. Photograph of typical projectile and sabot components

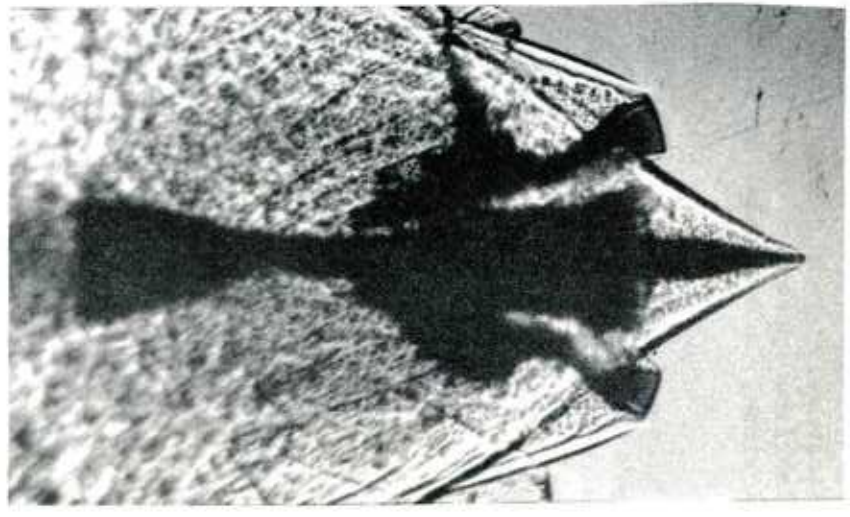

Figure 2a. Spark shadowgraph of discard flow field

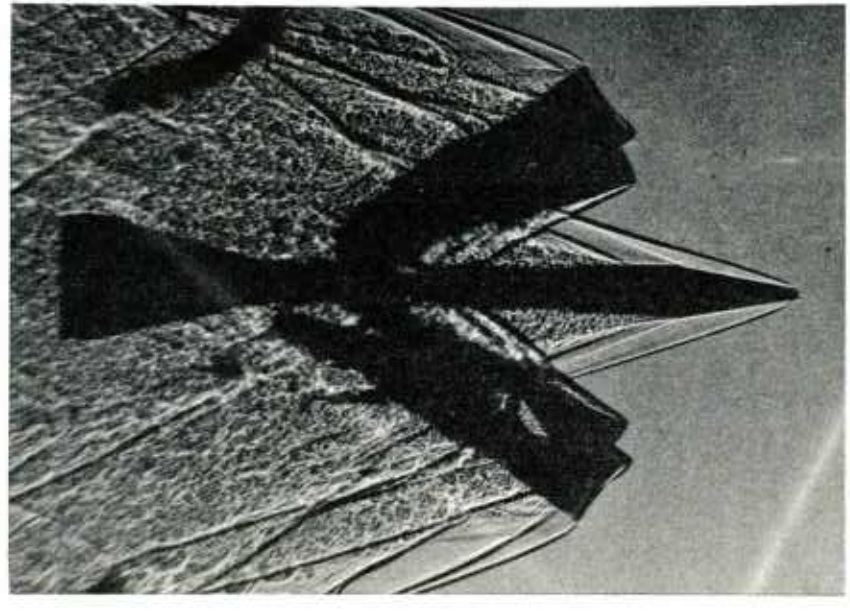

Figure 2b. Spark shadowgraph of discard flow field

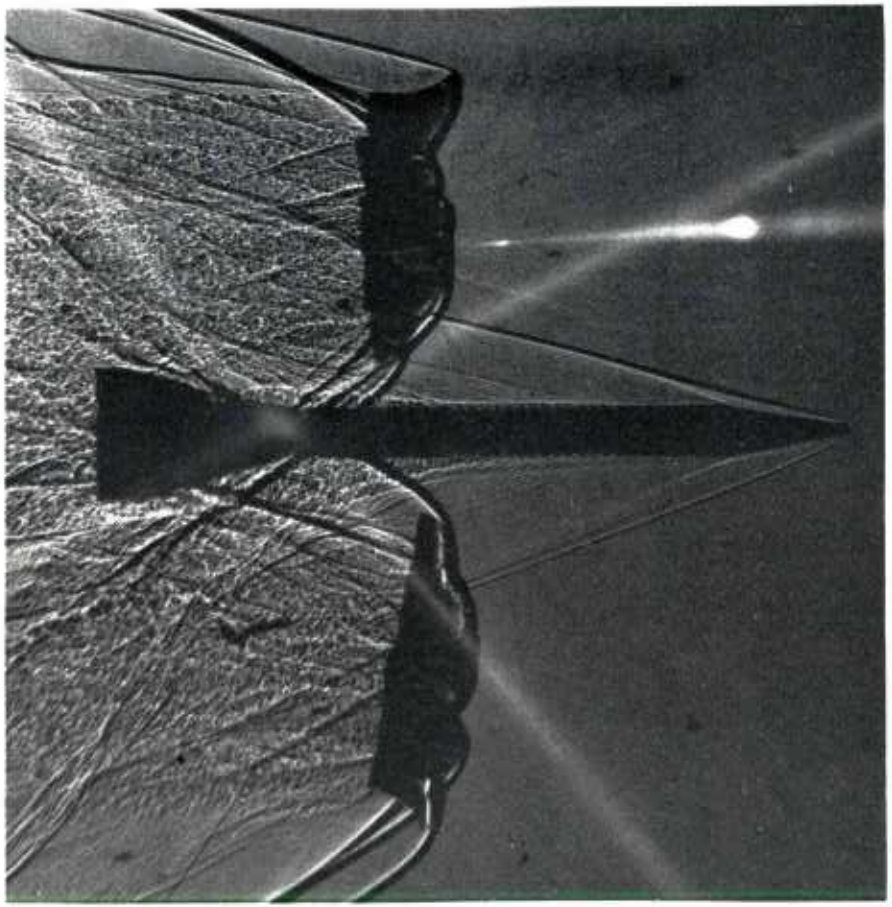

Figure 2c. Spark shadowgraph of discard flow field

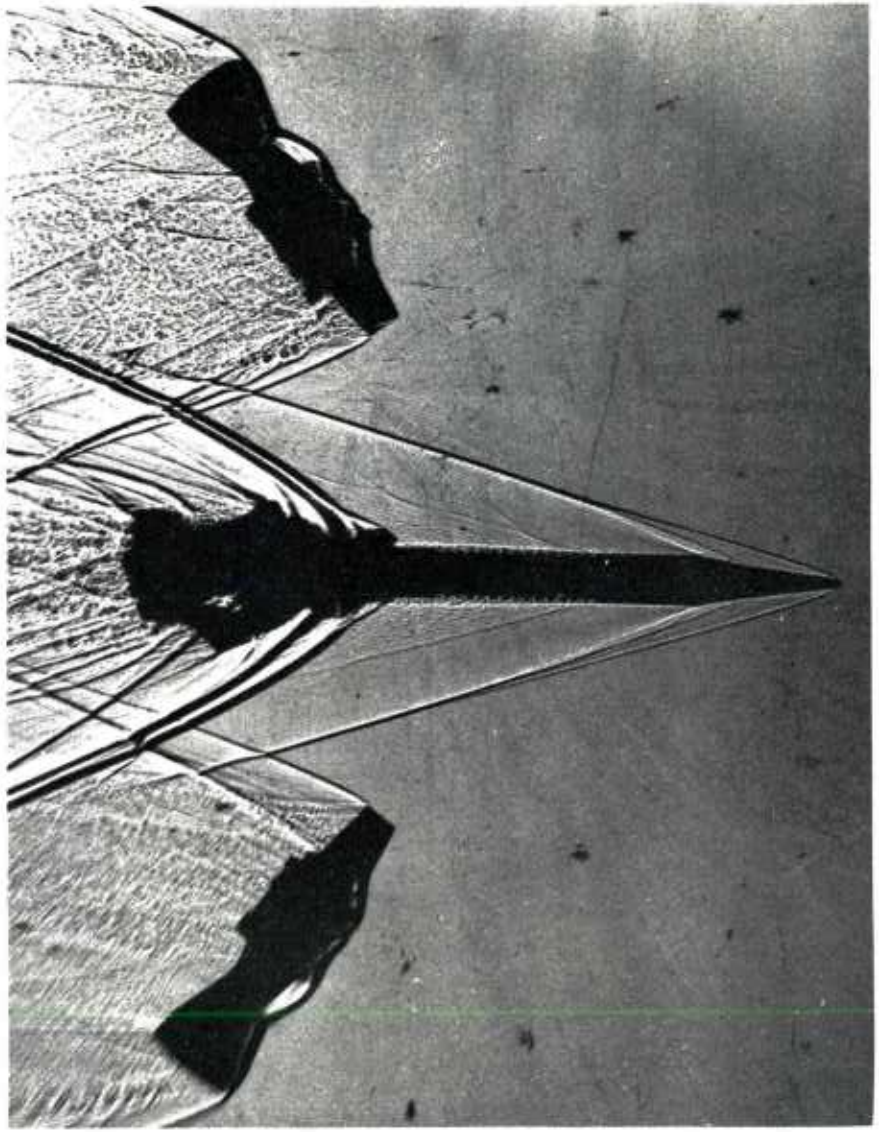

Figure 2d. Spark shadowgraph of discard flow field

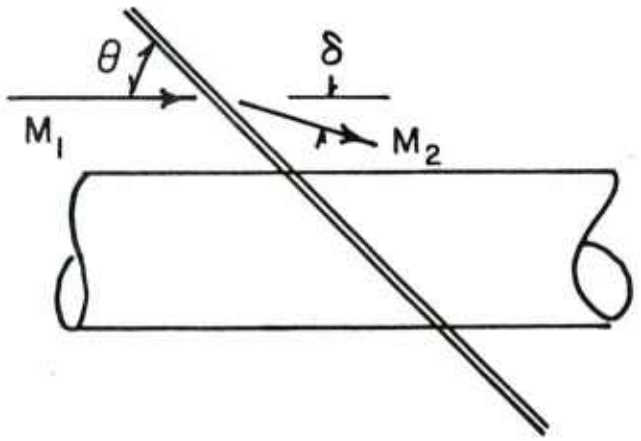

FIG.(3) SCHEMATIC OF A PLANE SHOCK INTERSECTING A CYLINDER

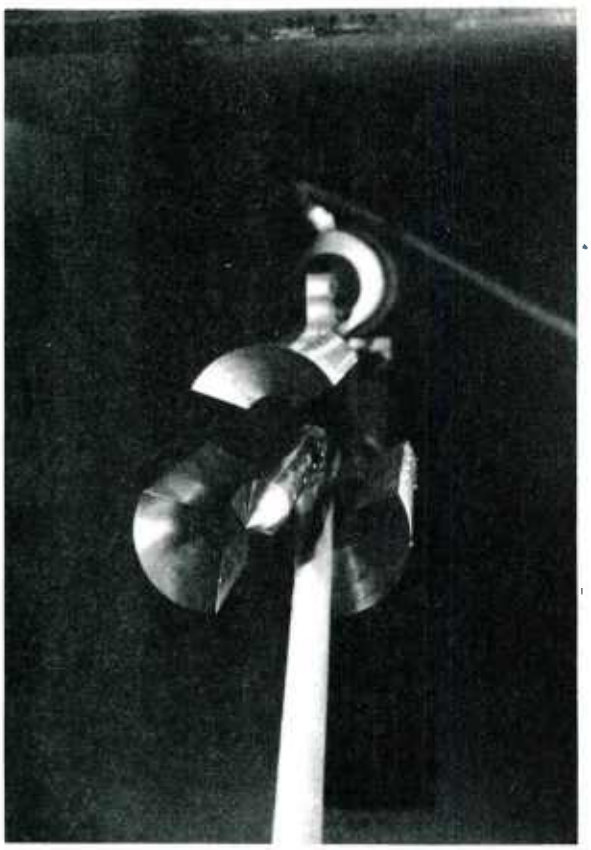

FIG.(4a) PROJECTILE WITH THREE SABOT COMPONENTS MOUNTED IN WIND TUNNEL

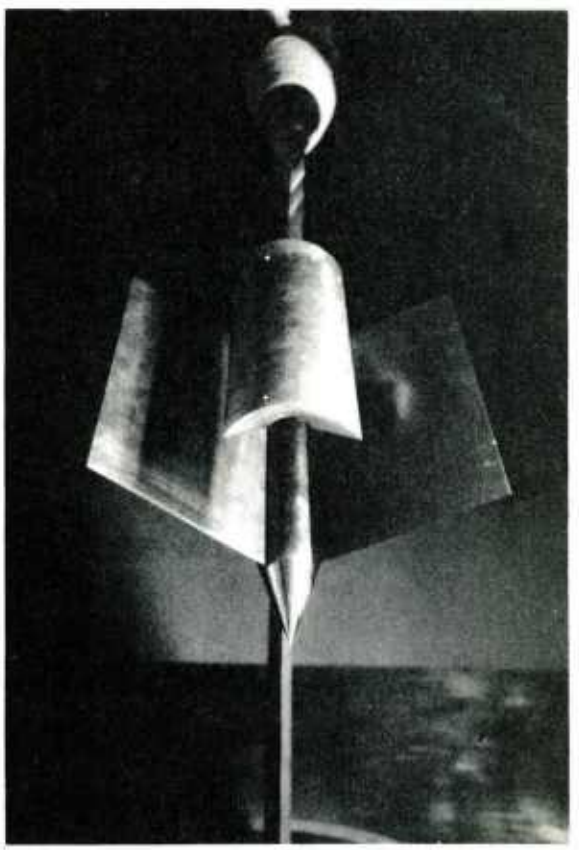

FIG.(4b) PROJECTILE WITH SABOT AND SPLITTER PLATES MOUNTED IN WIND TUNNEL

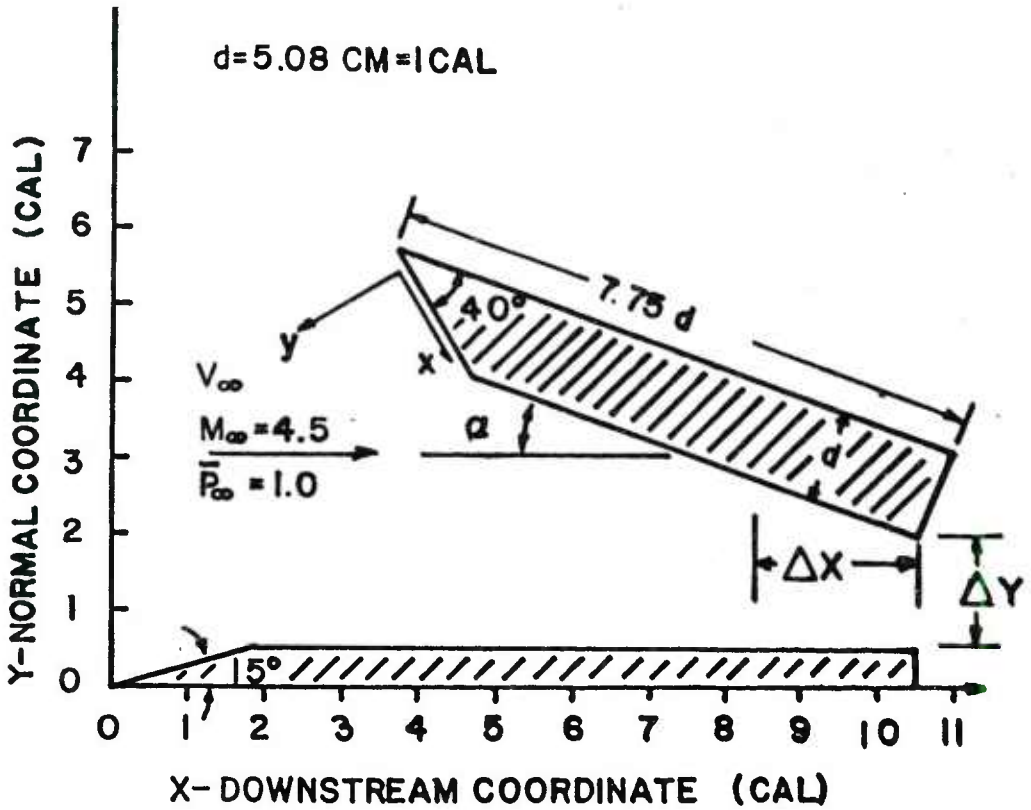

FIG.(5) TEST AND COMPUTATIONAL COORDINATE SYSTEMS

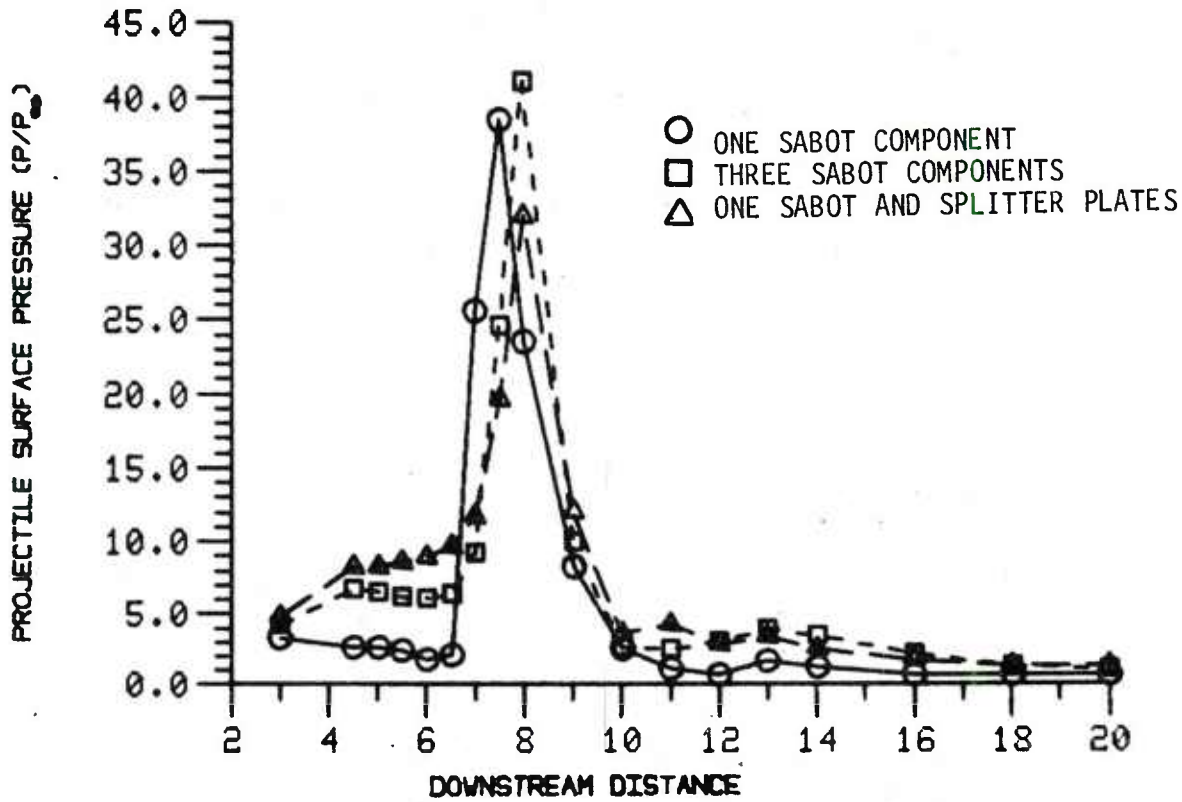

FIG.(6) PROJECTILE SURFACE PRESSURE DISTRIBUTIONS FOR SABOTS LOCATED IN THE "SYMMETRY CASE" (X/D = 0.0 , α =0.0°, ϕ =0.0°)

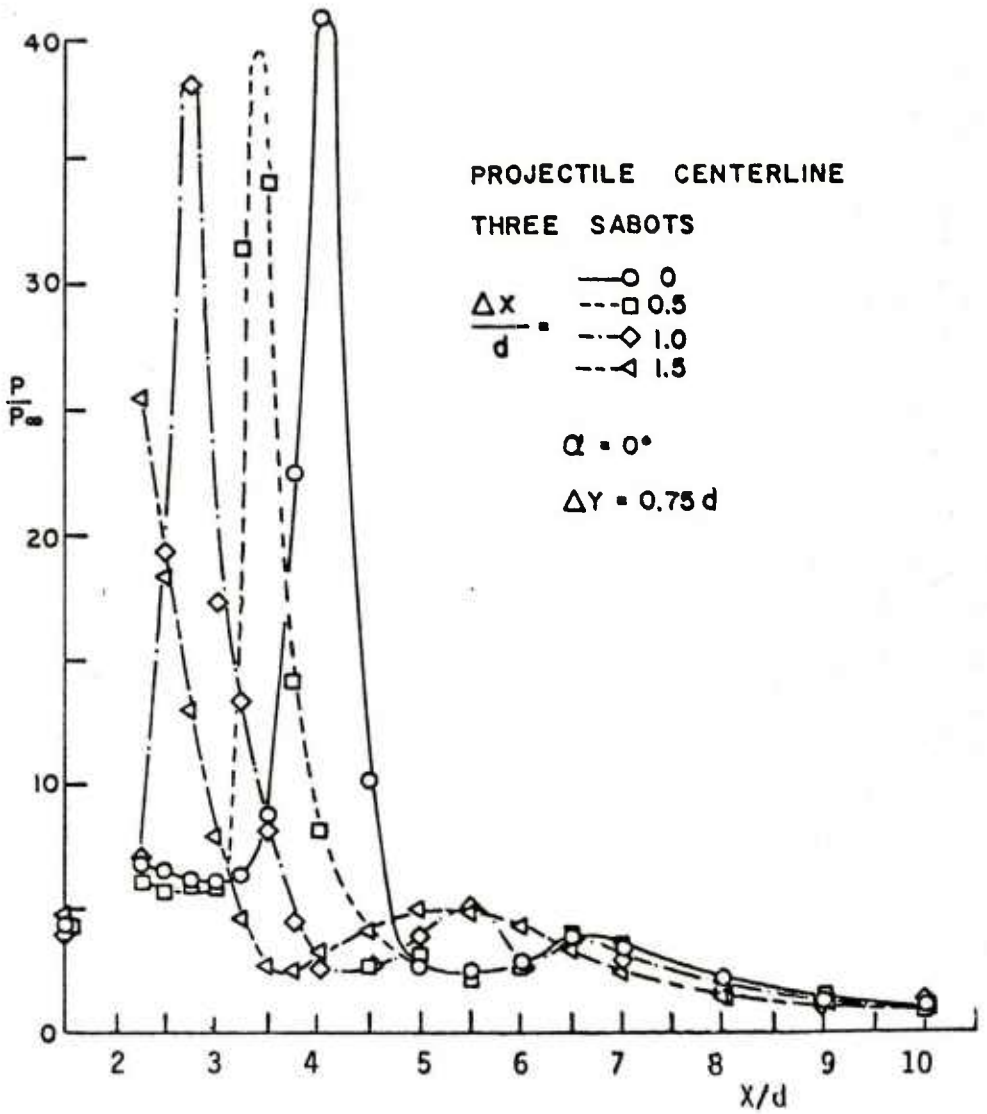

FIG.(7) PROJECTILE PRESSURE DISTRIBUTION WITH THREE SABOT COMPONENTS INSTALLED, ONE OF WHICH IS BEING TRAVERSED FORWARD

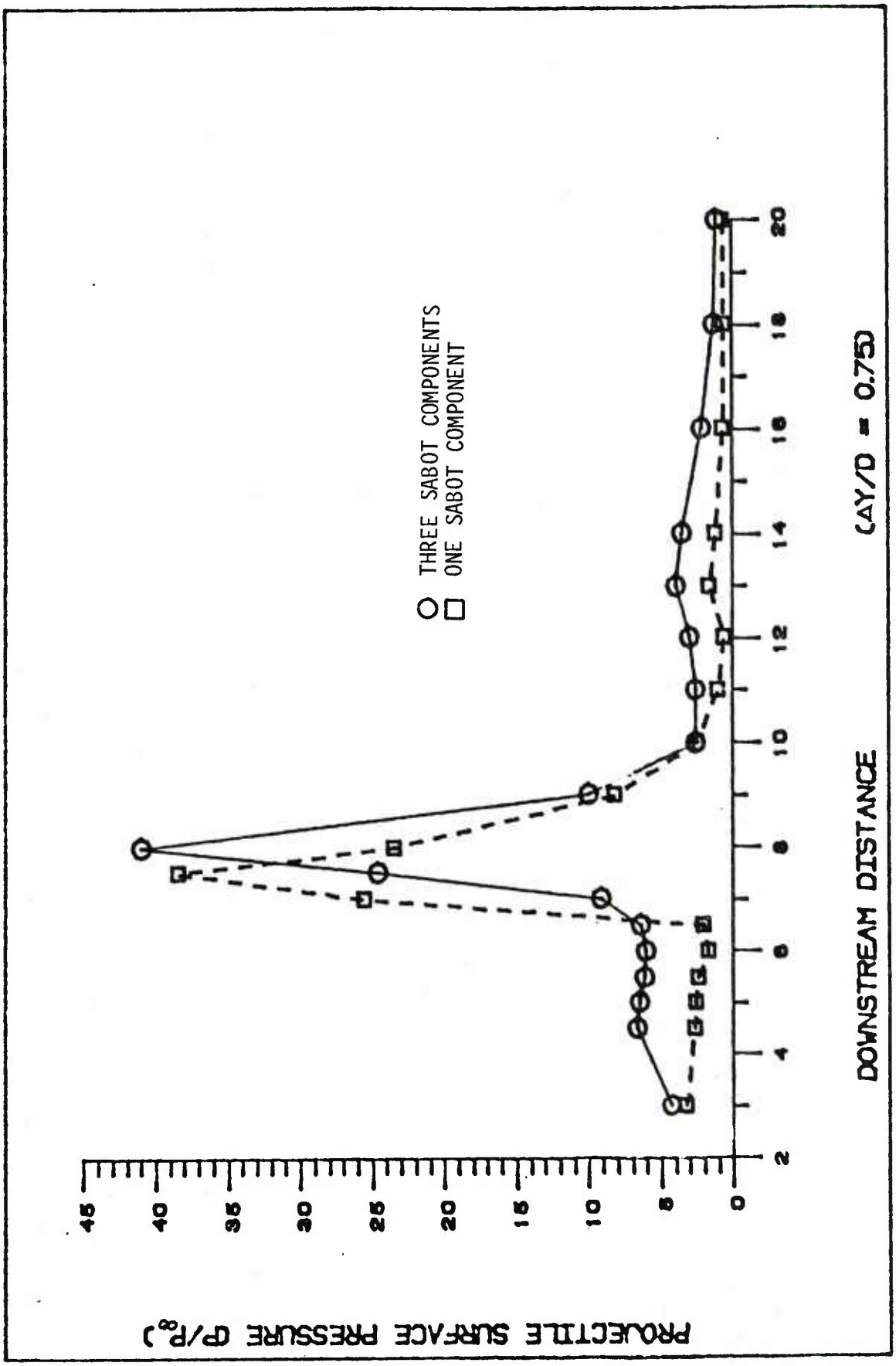

FIG.(8) COMPARISON OF PERIPHERAL VARIATION IN PRESSURE DISTRIBUTION WITH ONE AND THREE SABOT COMPONENTS MOUNTED IN THE "SYMMETRY" POSITION ($\phi = 0.0^{\circ}$)

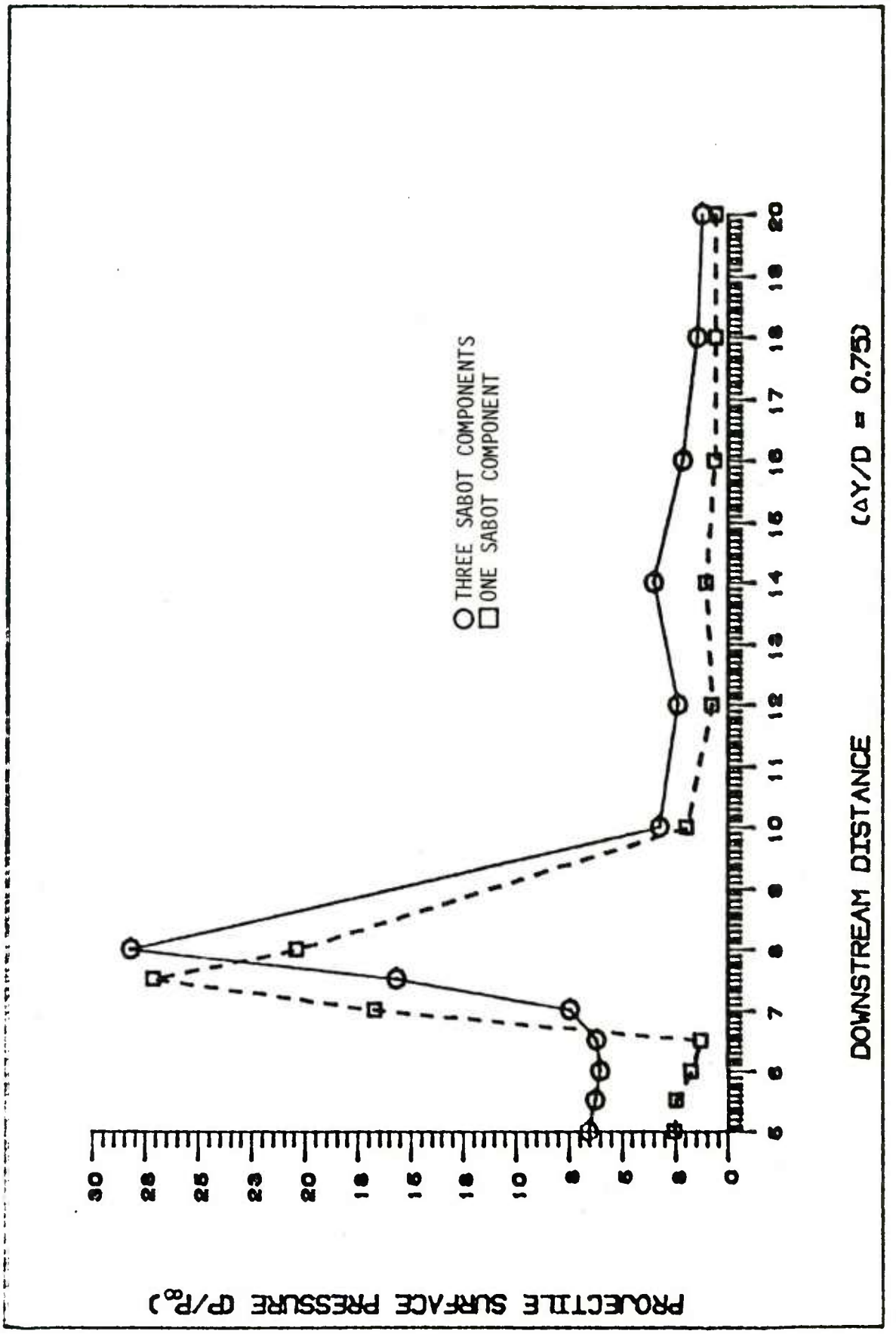

FIG.(8) CONTINUED (ϕ = 30.0°)

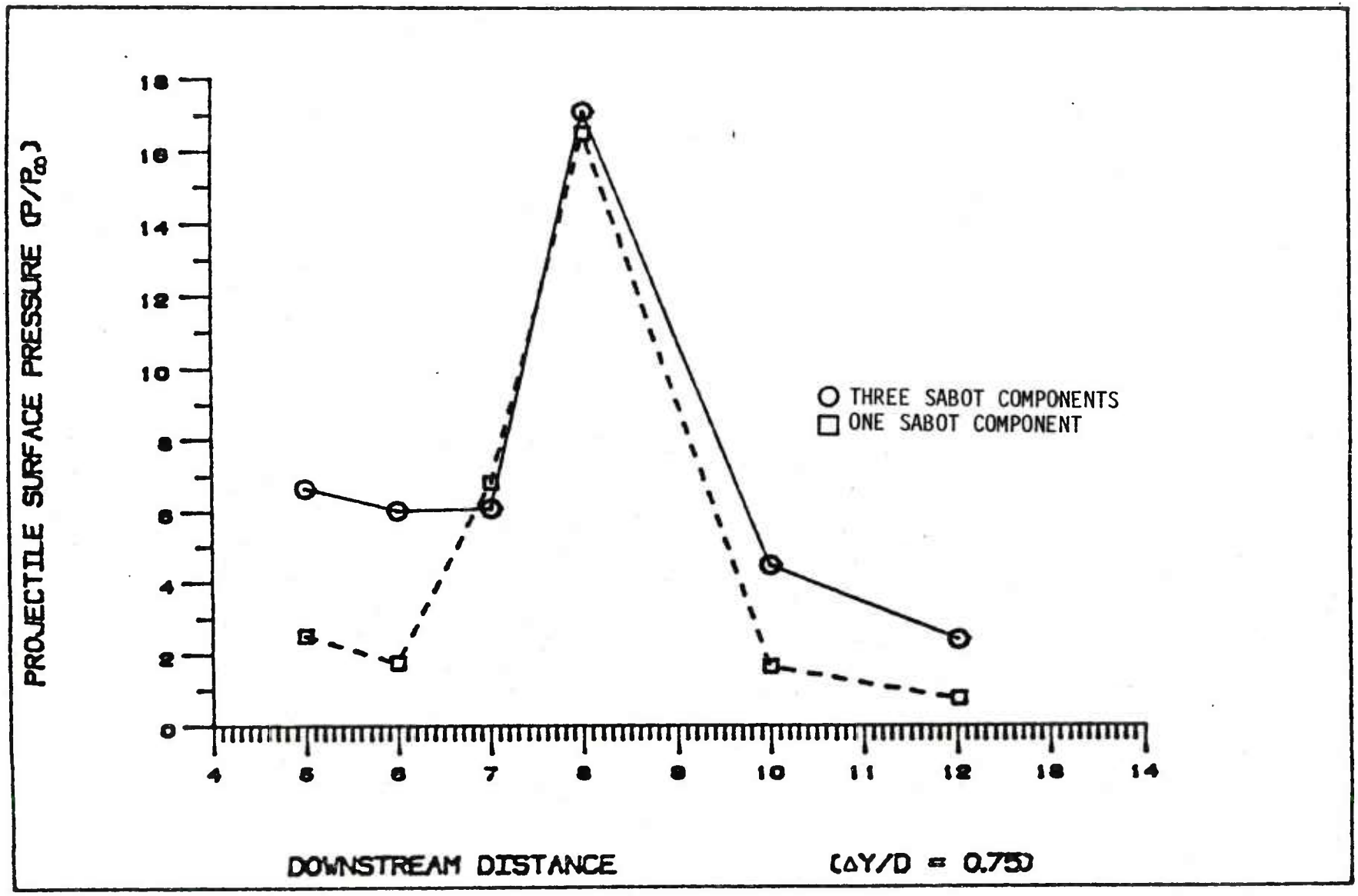

FIG.(8) CONTINUED (ϕ = 45.0°)

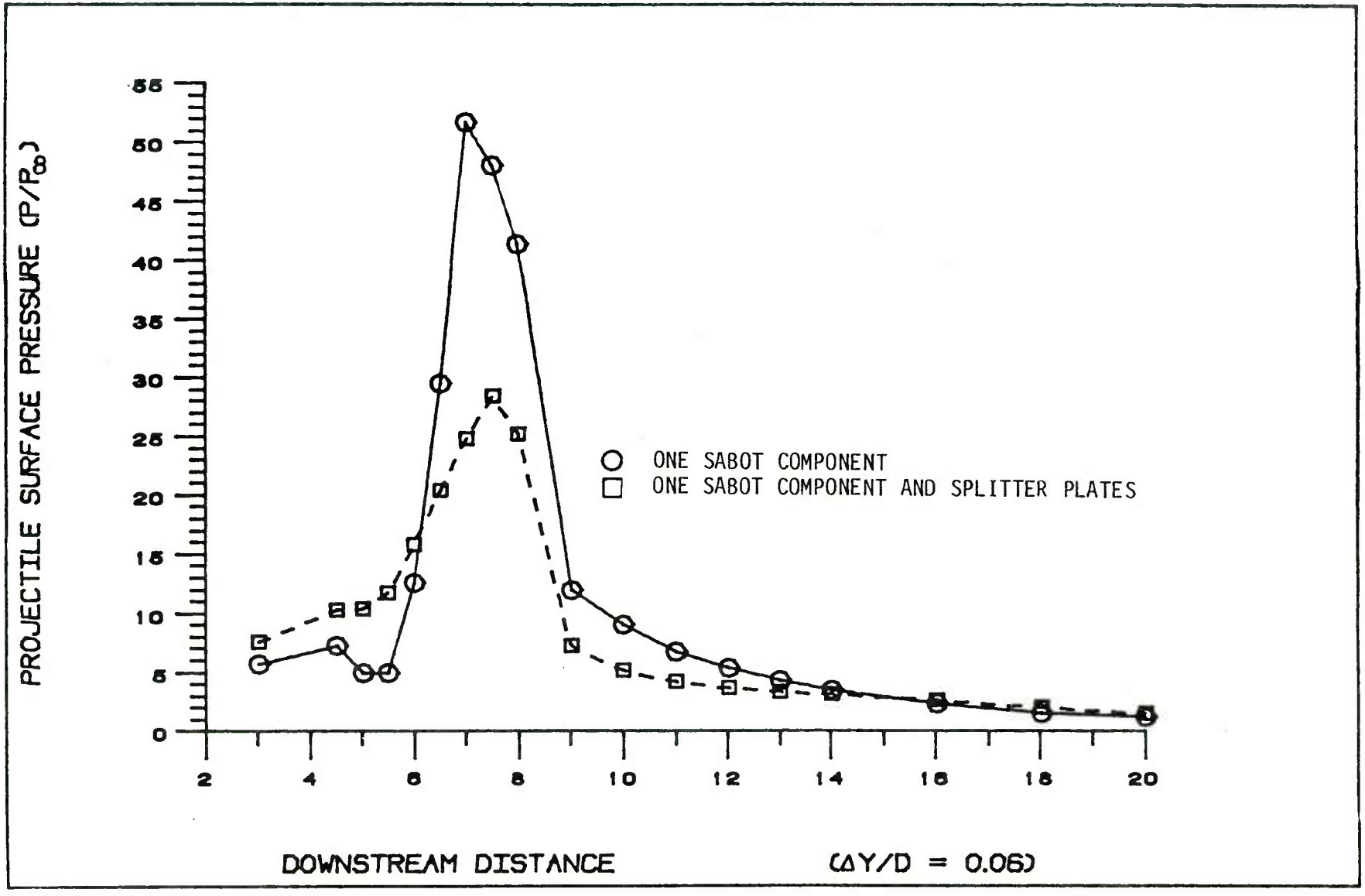

FIG.(9) PROJECTILE CENTERLINE PRESSURE DISTRIBUTION FOR DIFFERENT SABOT SEPARATIONS (α = 0.0°)

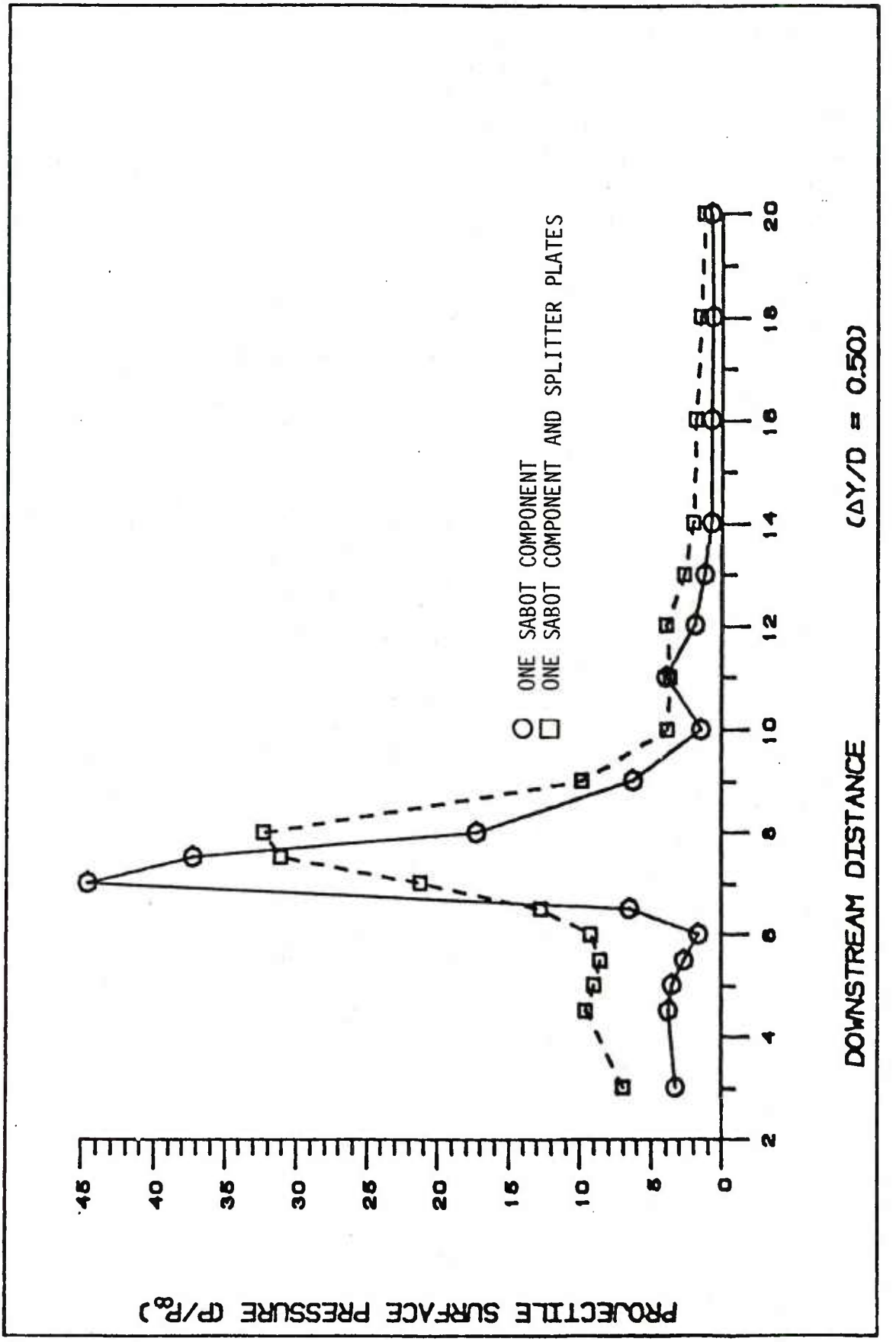

FIG.(9) CONTINUED

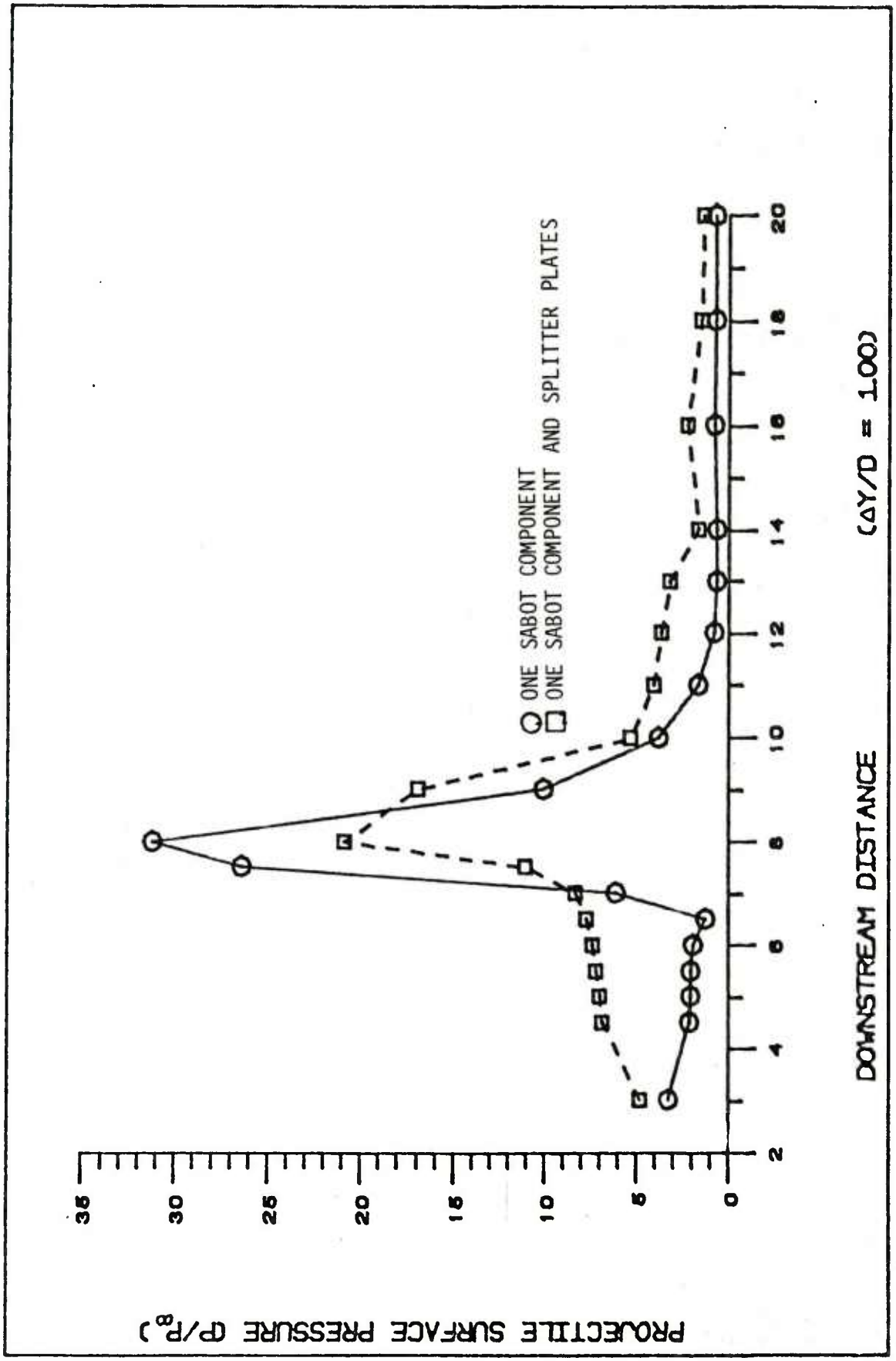

FIG.(9) CONTINUED

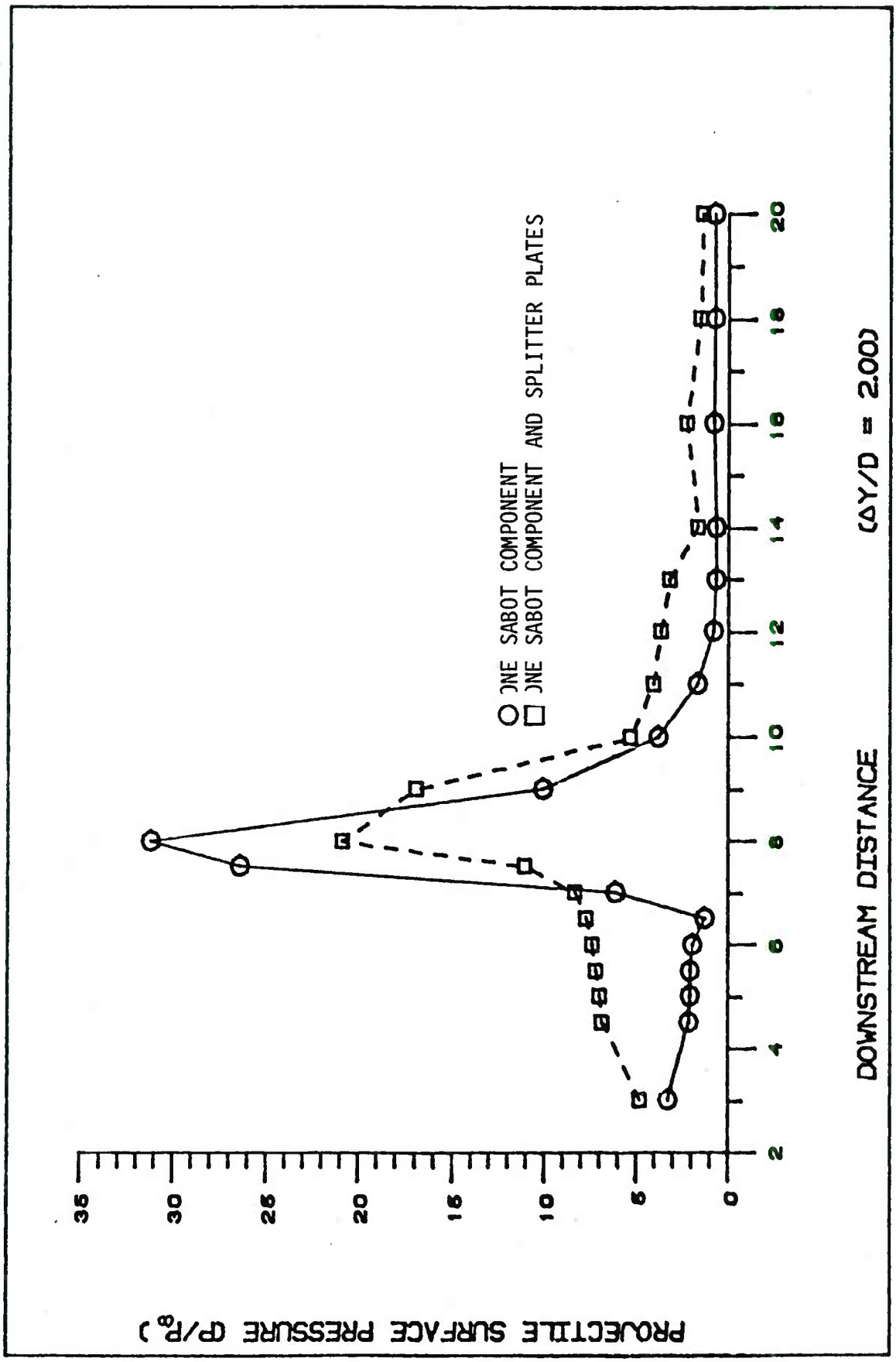

FIG.(9) CONTINUED

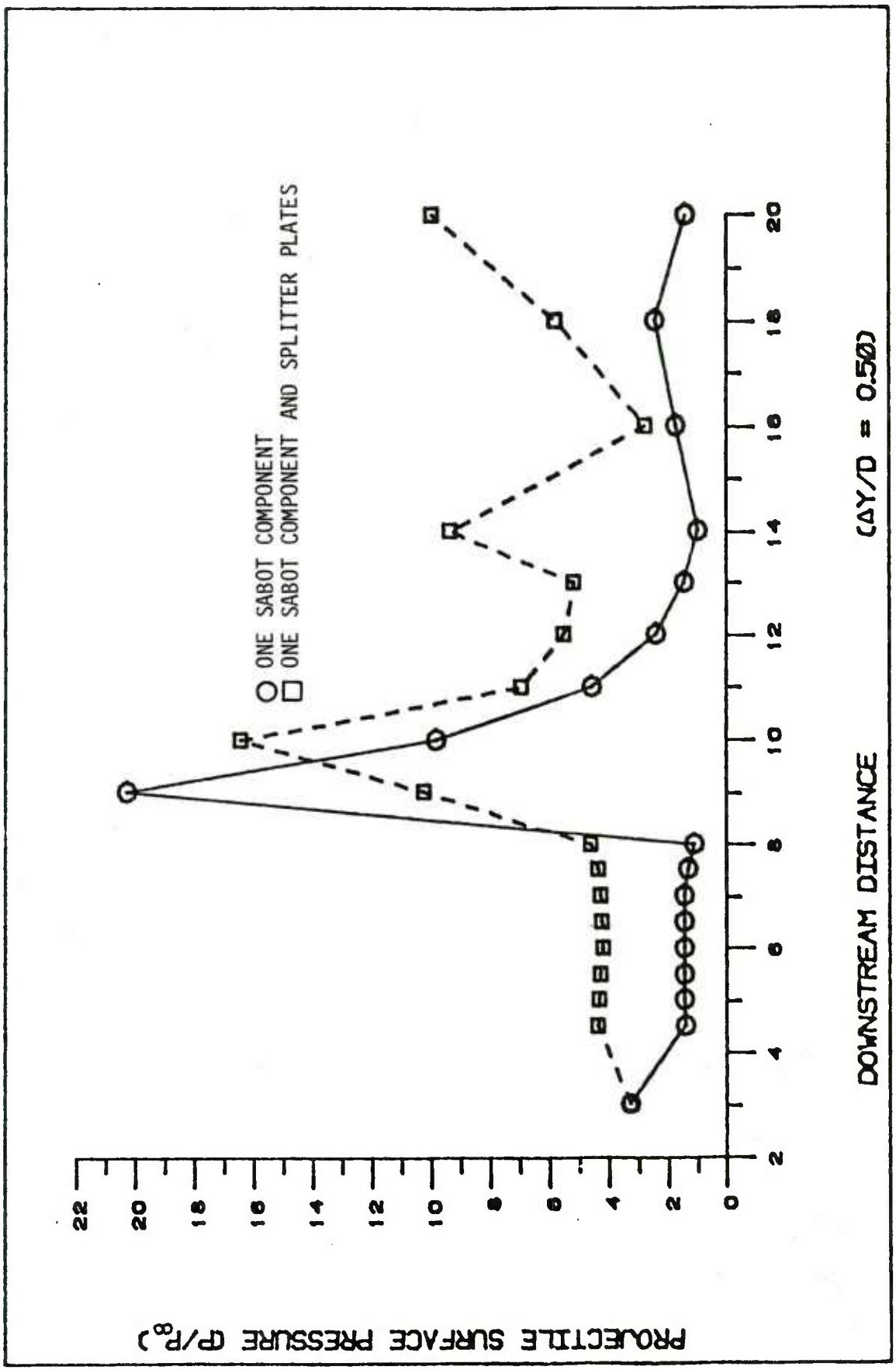

FIG.(10) PROJECTILE CENTERLINE PRESSURE DISTRIBUTION FOR DIFFERENT SABOT SEPARATIONS (α = 10.0°)

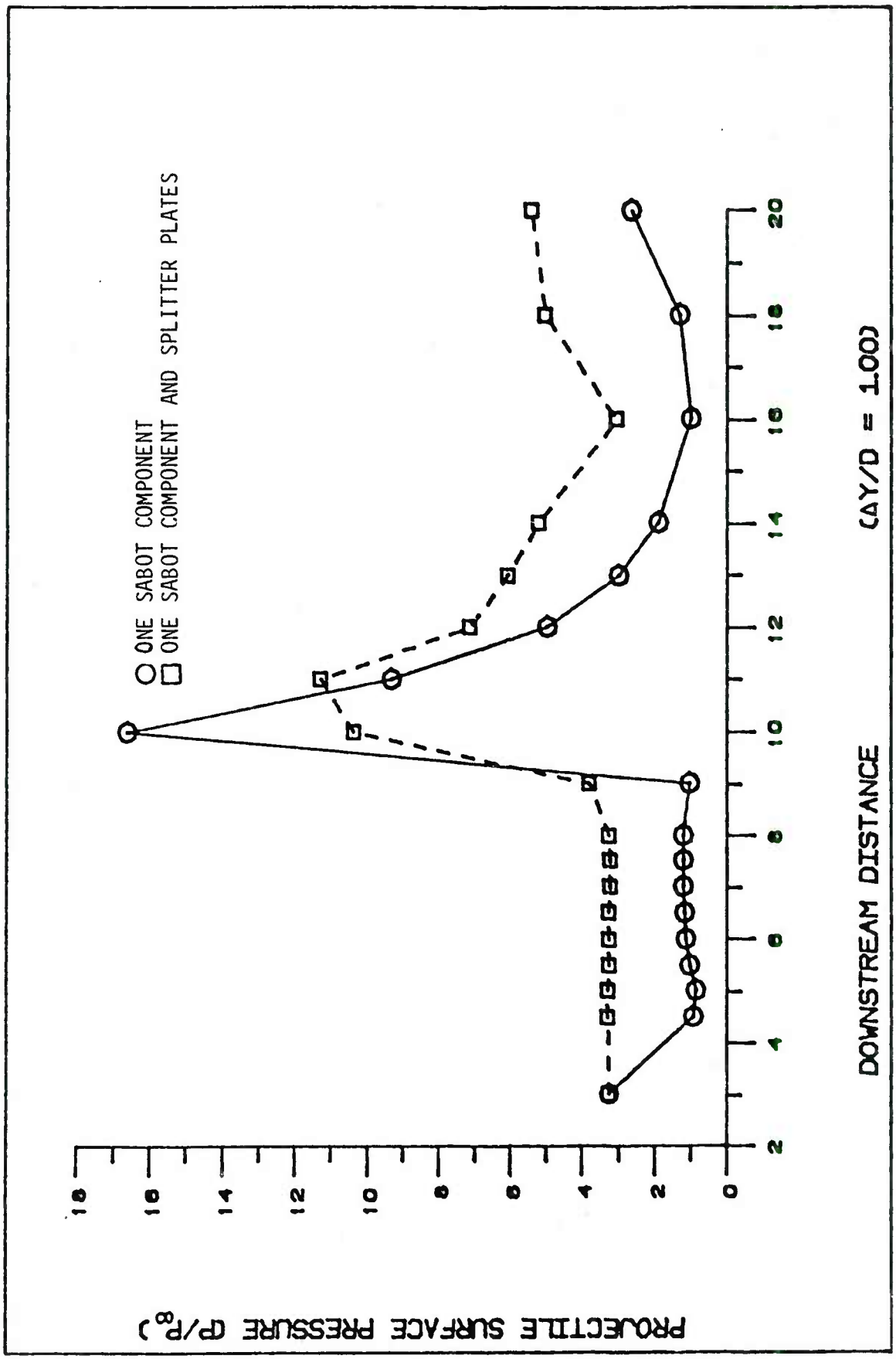

FIG.(10) CONTINUED

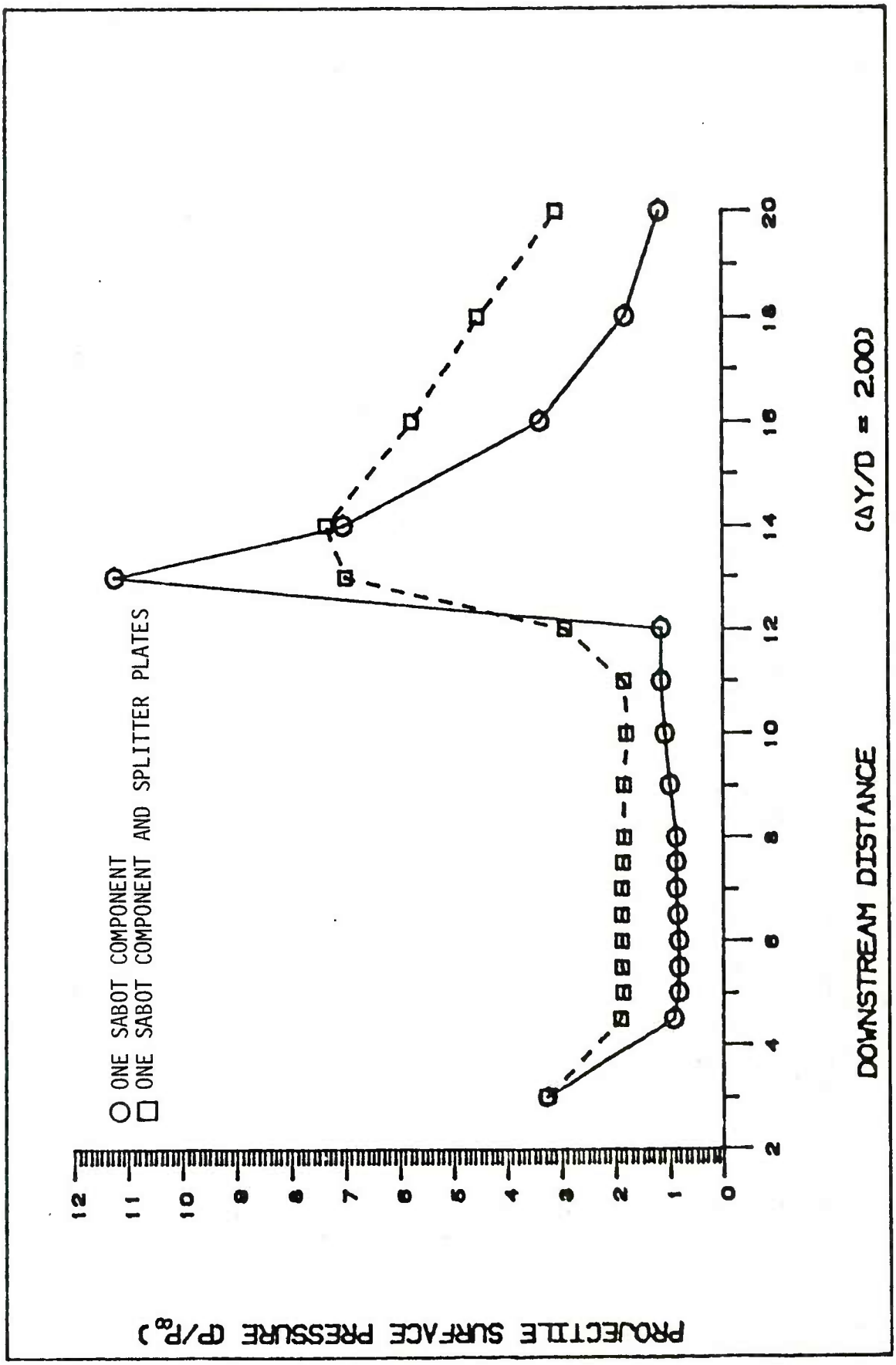

FIG.(10) CONTINUED

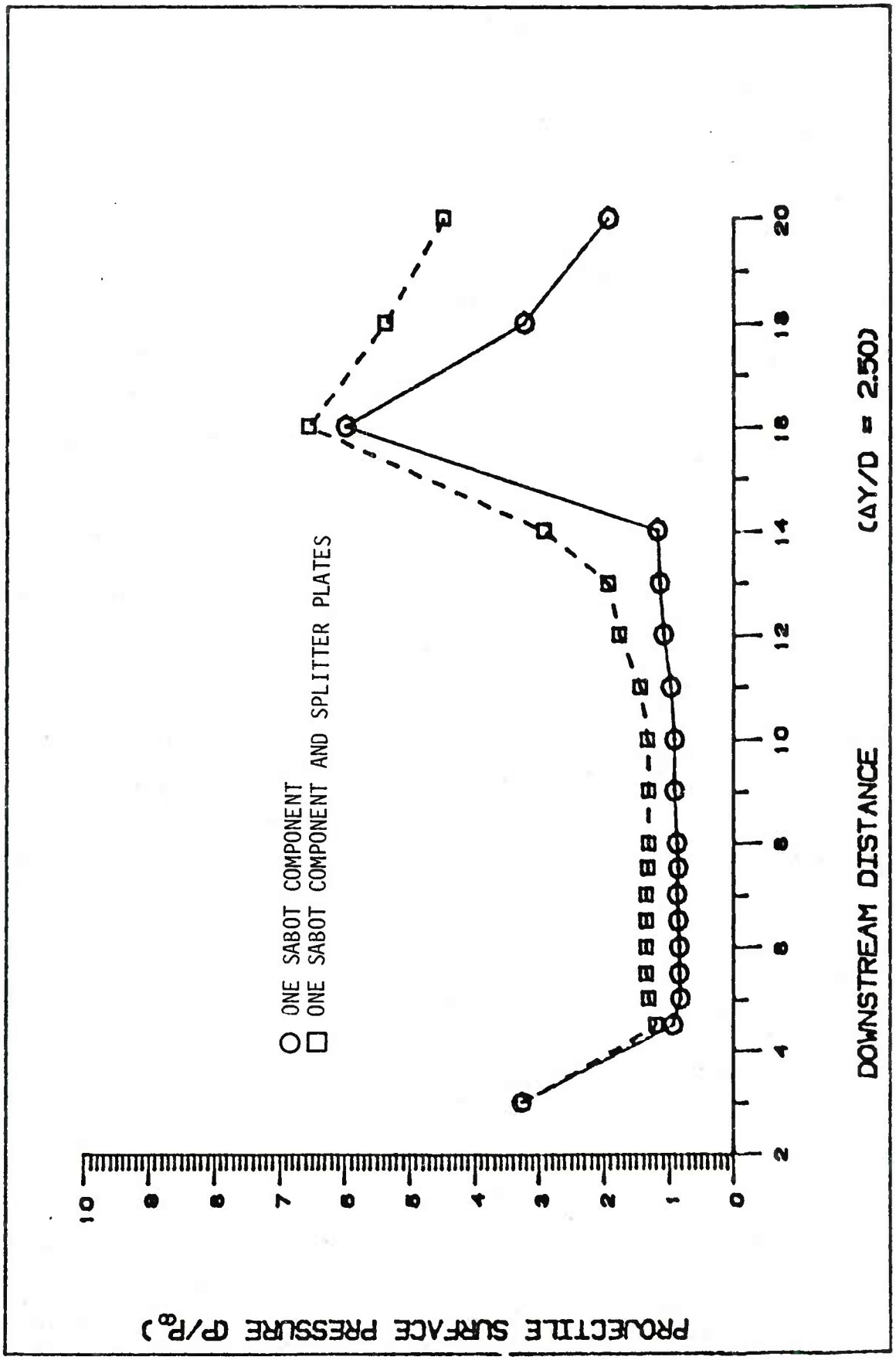

FIG.(10) CONTINUED

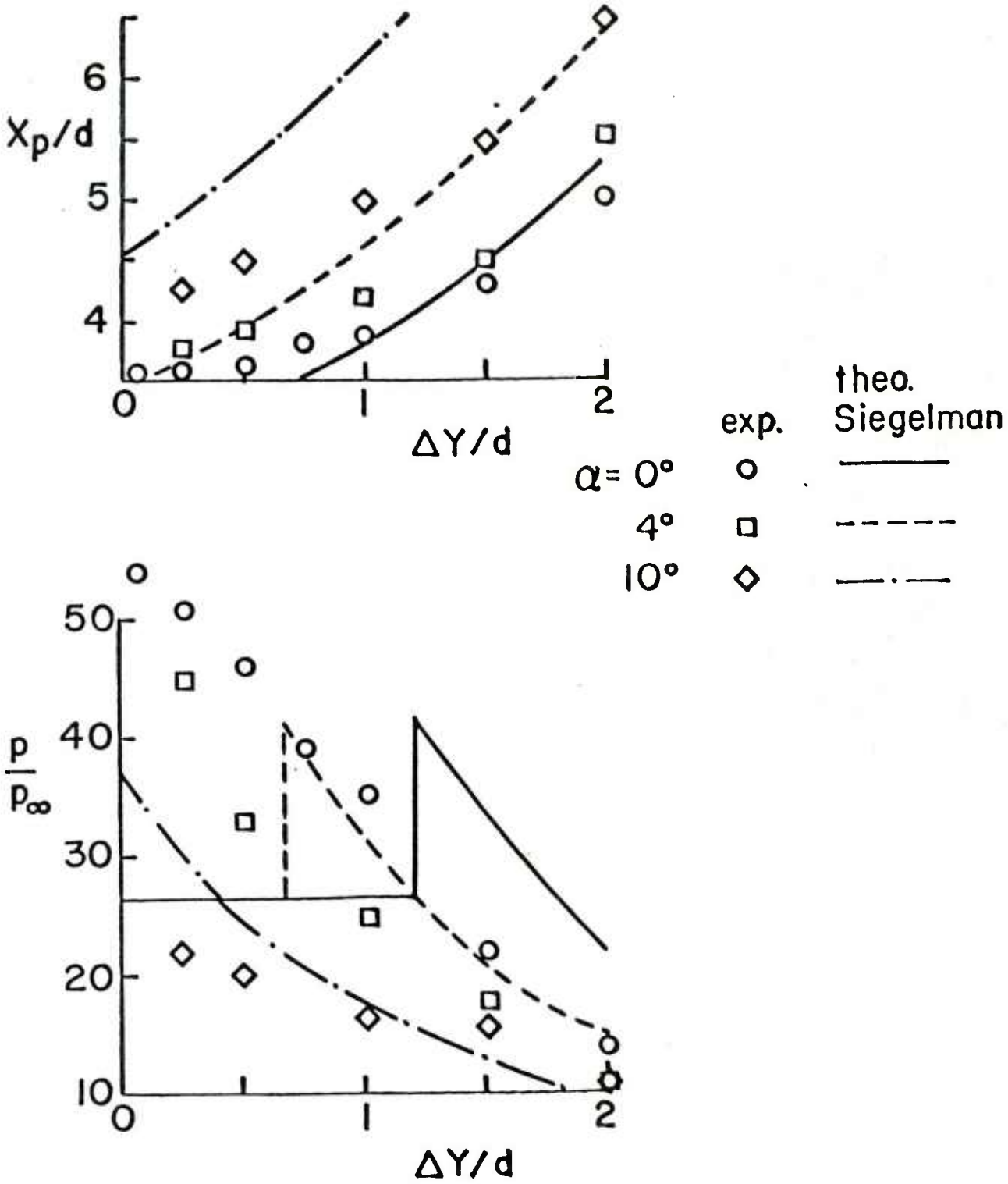

FIG.(11a) COMPARISON OF MEASURED AND PREDICTED PROPERTIES FOR PEAK PRESSURE LOCATION ON THE PROJECTILE SURFACE: CASE FOR ONE SABOT COMPONENT

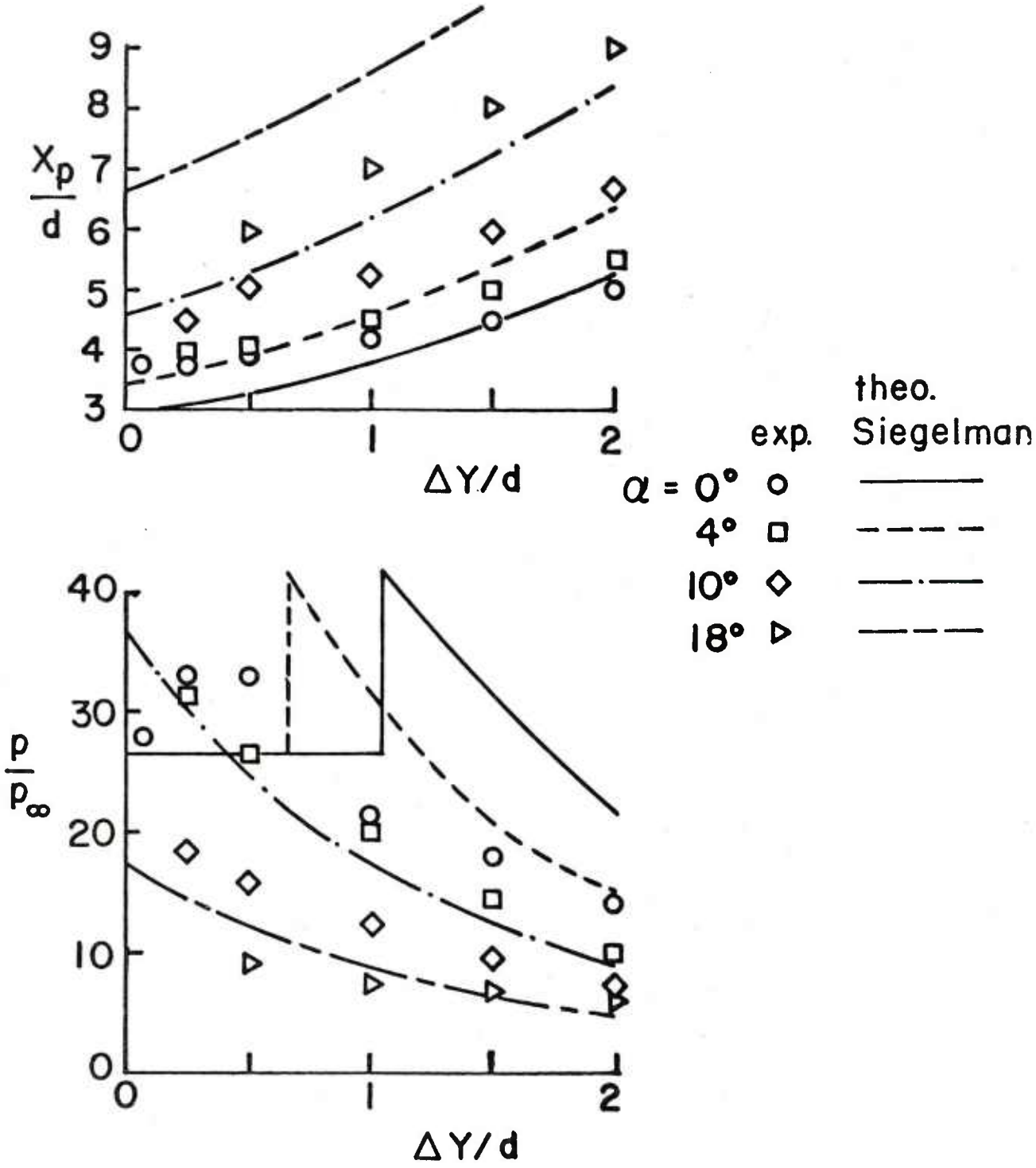

FIG.(11b) COMPARISON OF MEASURED AND PREDICTED PROPERTIES FOR PEAK PRESSURE LOCATION ON THE PROJECTILE SURFACE: CASE FOR ONE SABOT COMPONENT AND SPLITTER PLATES

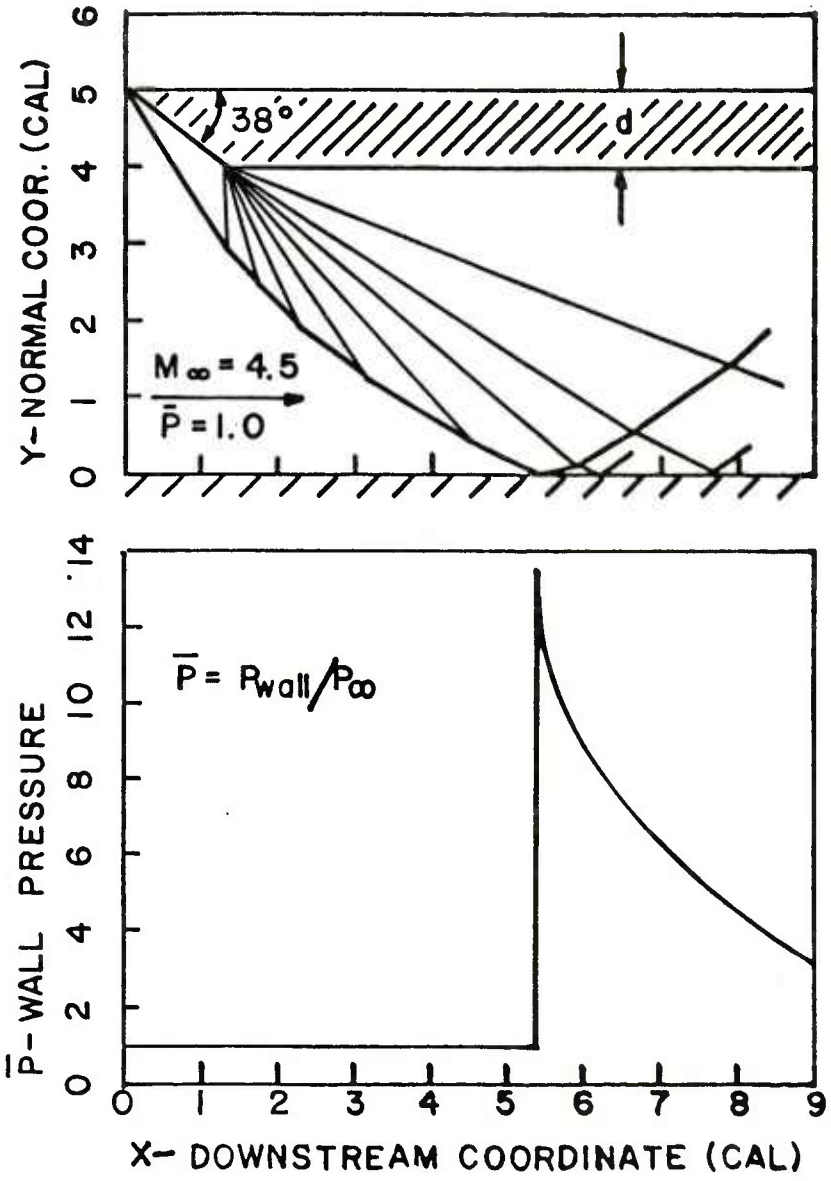

FIG.(12) WAVE PATTERNS IN TWO-DIMENSIONAL ANALOG OF SABOT/PROJECTILE INTERFERENCE

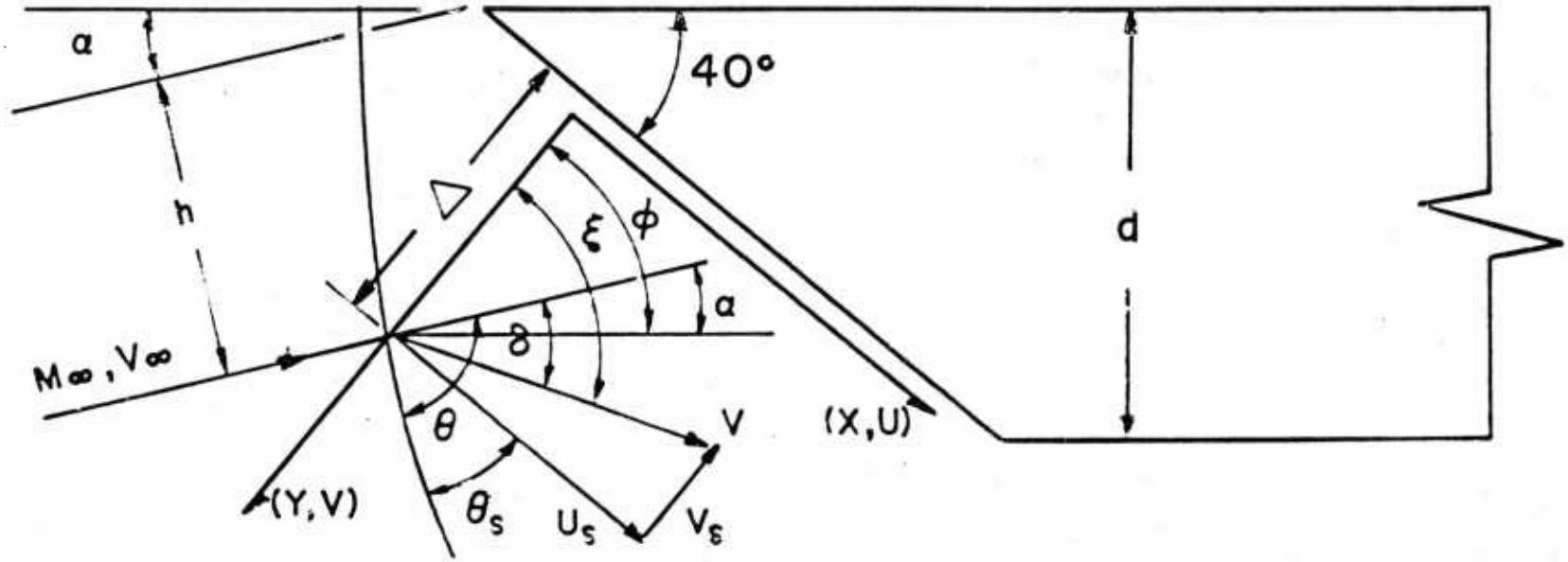

FRONT FACE $h = X \sin(40° + \alpha) + \Delta \sin(\phi - \alpha)$

DOWNSTREAM $h = X_{ff} \sin(40° + \alpha) + \Delta \sin(\phi - \alpha) + (X - X_{ff}) \sin \alpha$

FIG.(13) SABOT COORDINATE SYSTEM DETAIL

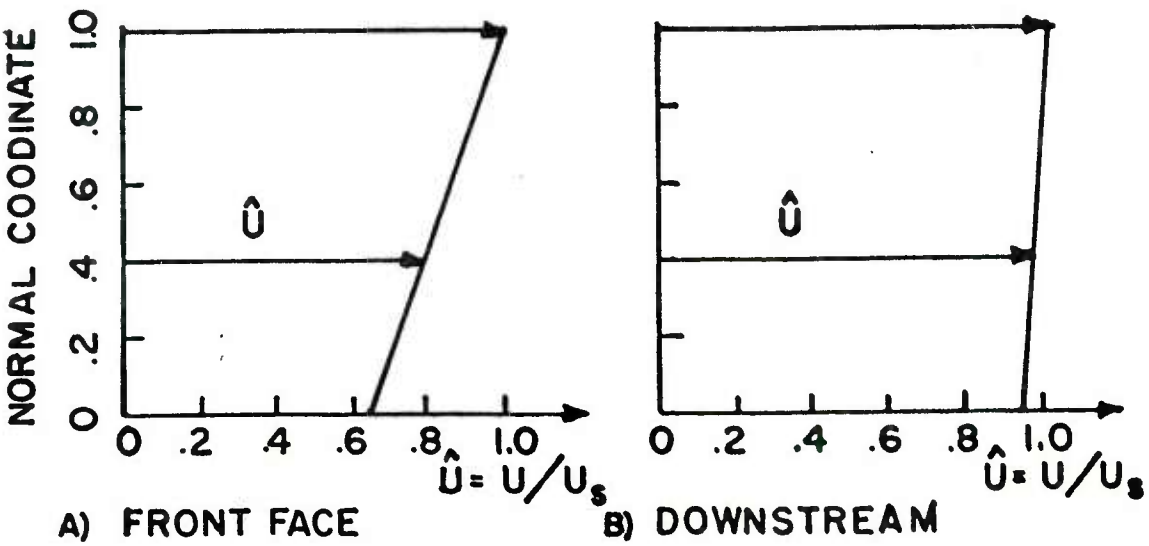

FIG.(14) SABOT SHOCK LAYER STREAMWISE VELOCITY PROFILES

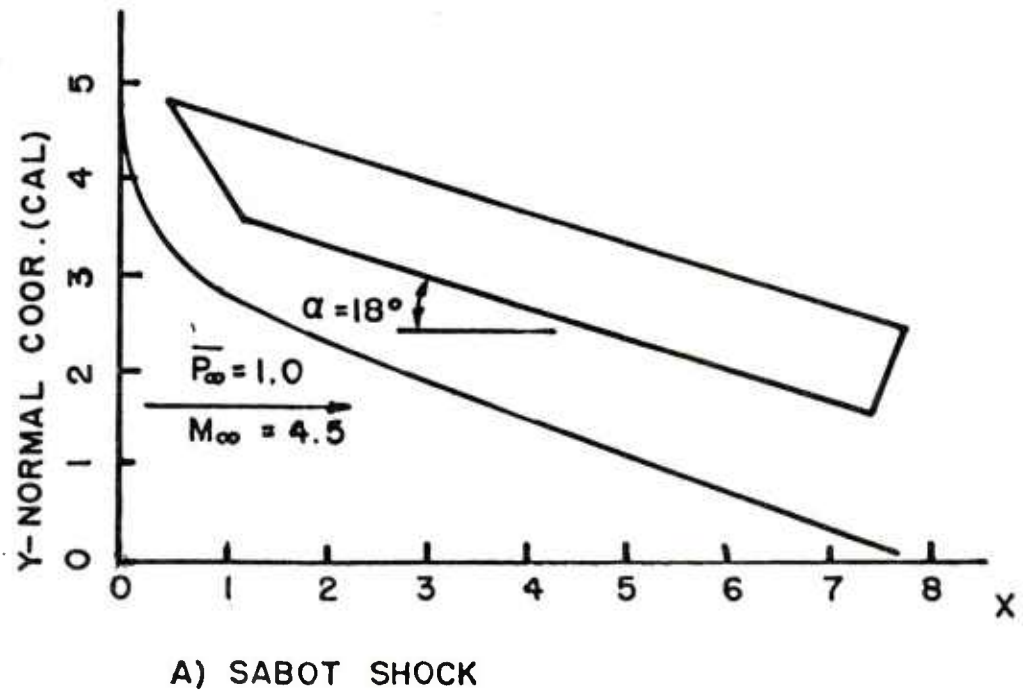

FIG.(15) TYPICAL COMPUTED SHOCK SHAPES

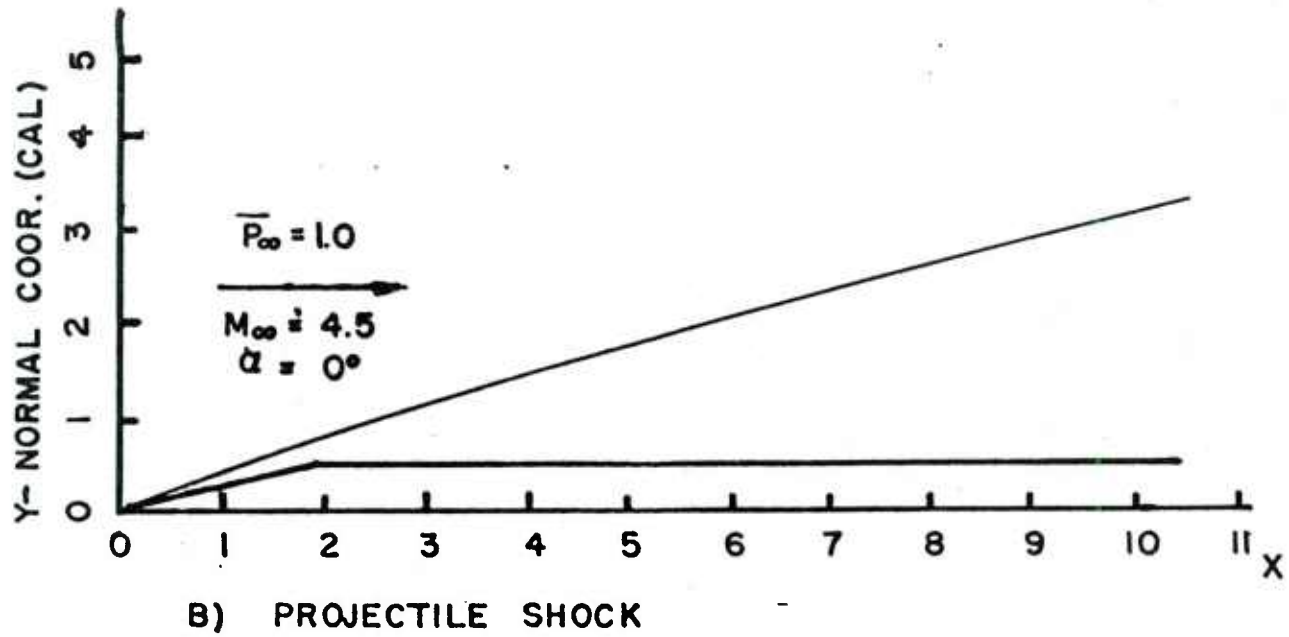

B) PROJECTILE SHOCK

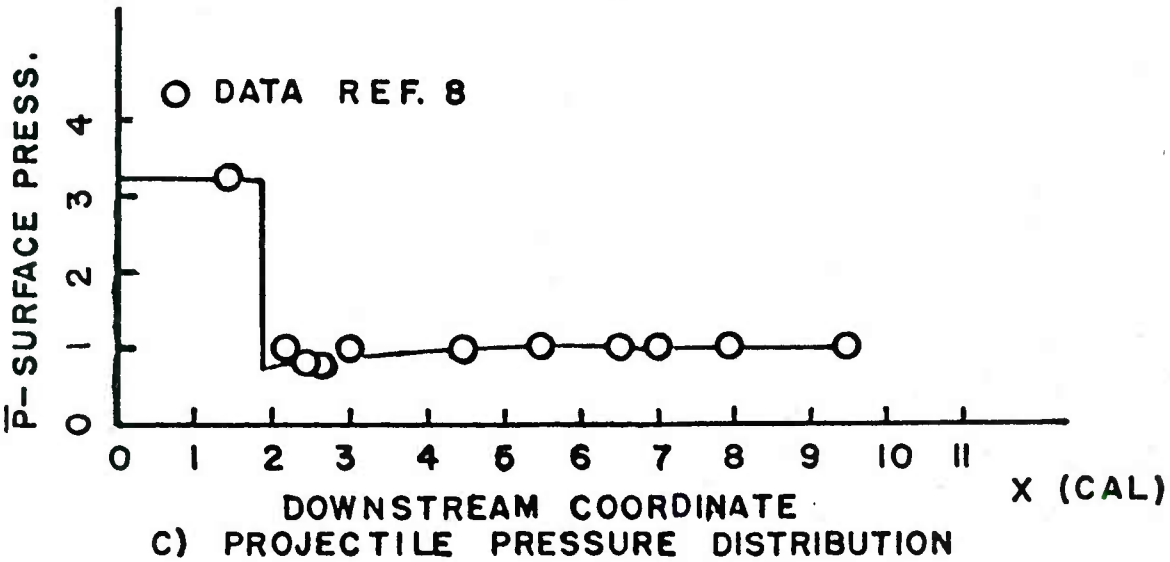

C) PROJECTILE PRESSURE DISTRIBUTION

FIG.(15) CONTINUED

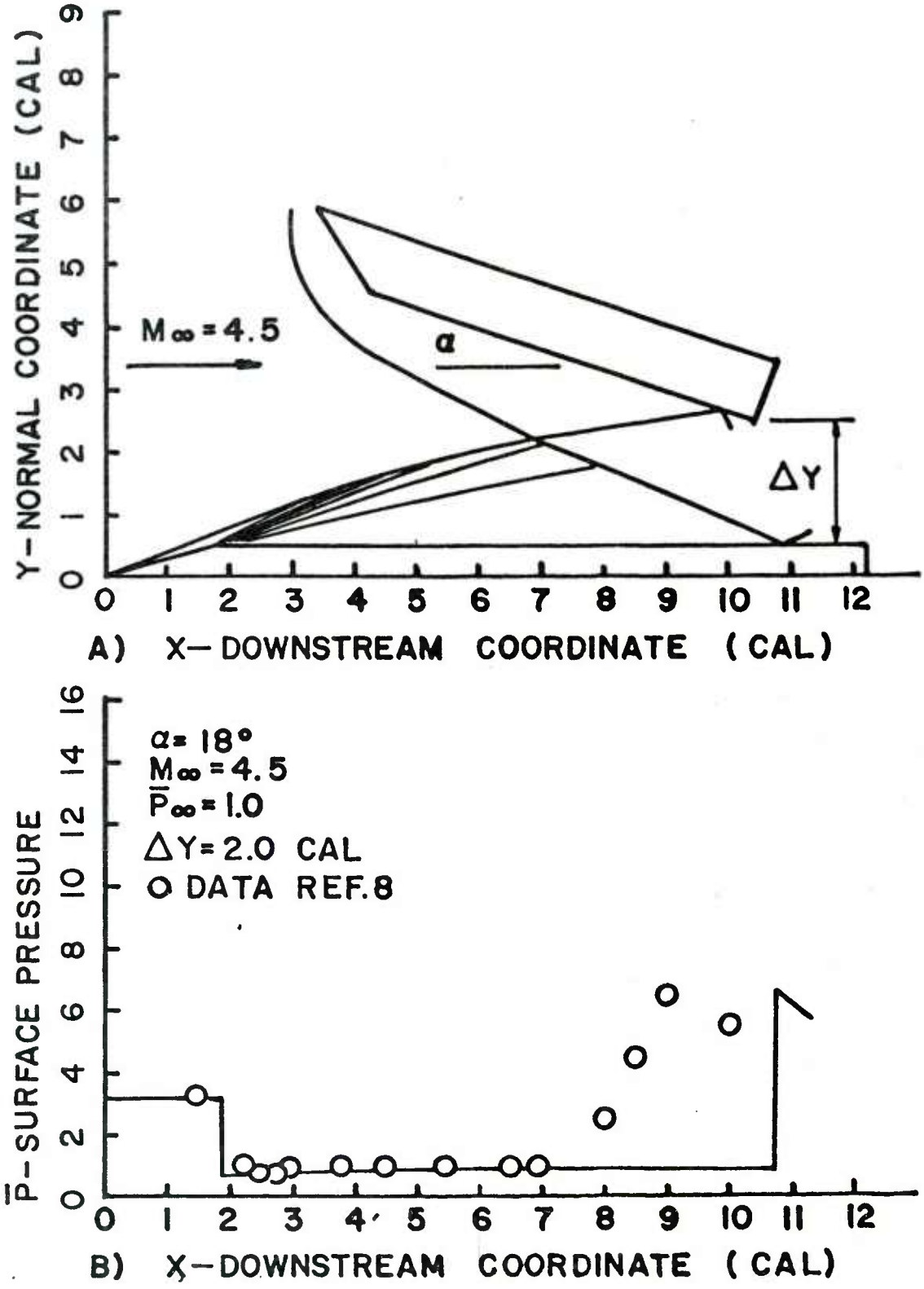

FIG.(16) INTERACTION WAVE PATTERN

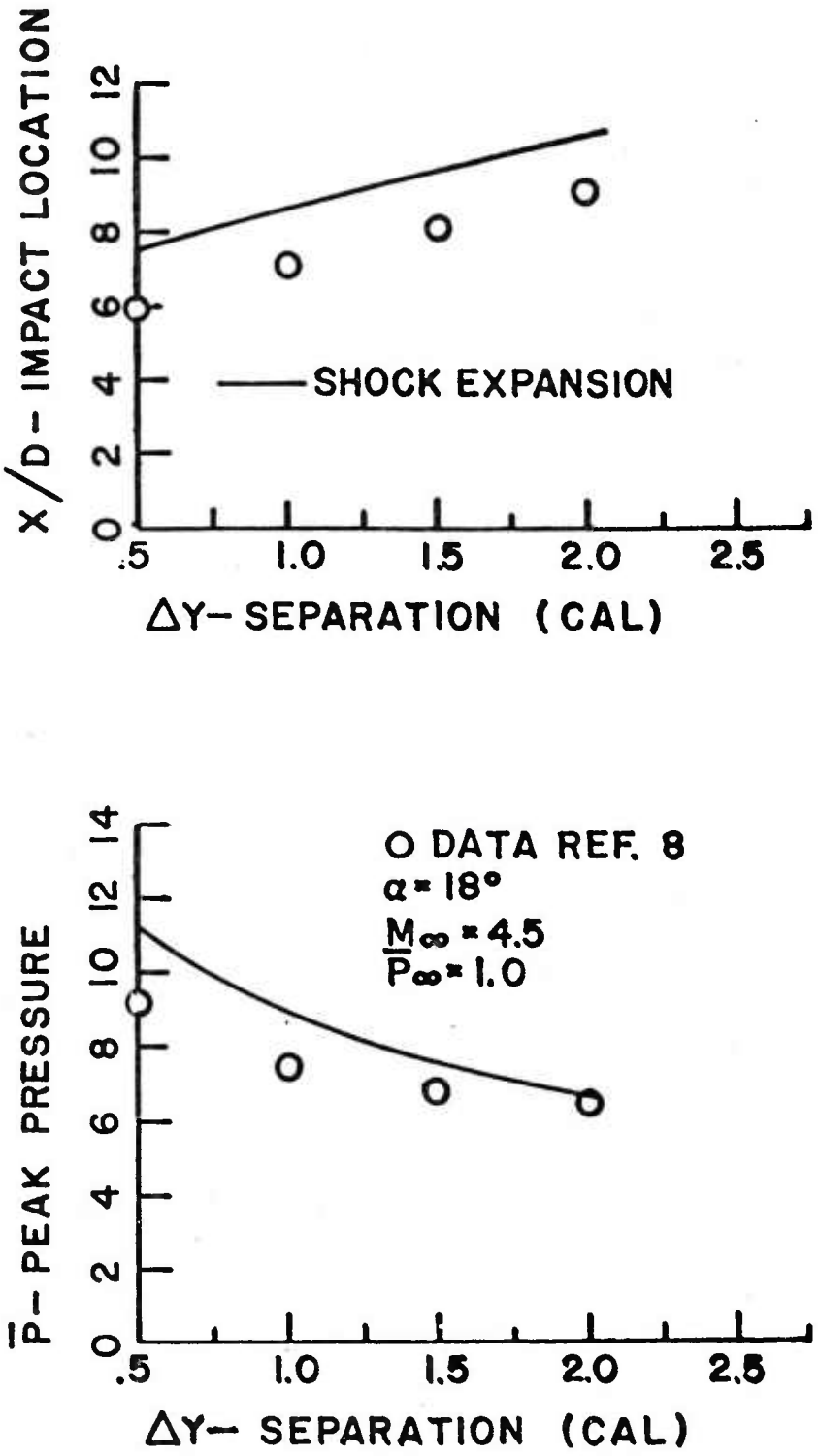

FIG.(17) PREDICTED IMPACT LOCATION AND PEAK PRESSURE LEVEL

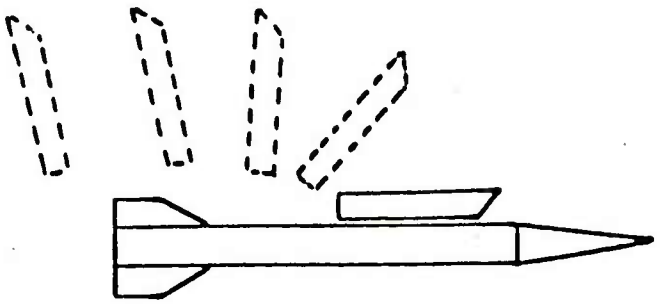

(A) DRAG DOMINATED SABOT

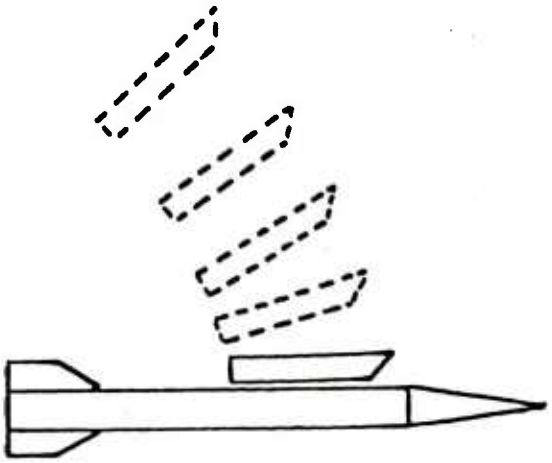

(B) LIFT DOMINATED SABOT

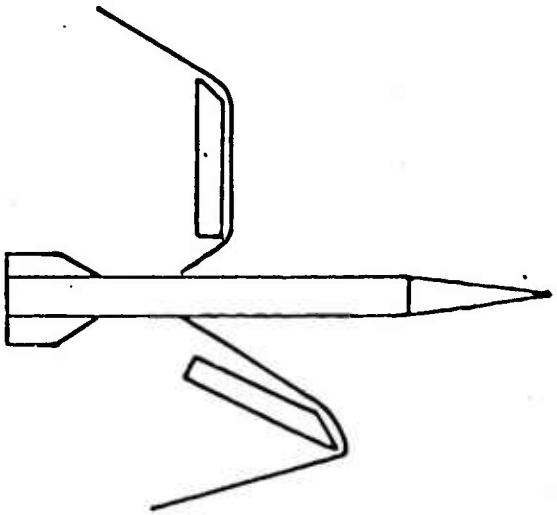

(C) MODEL OF DISCARD INTERACTION (t = 0.0)

FIG.(18) CONCEPTUAL SABOT DISCARD CATEGORIES

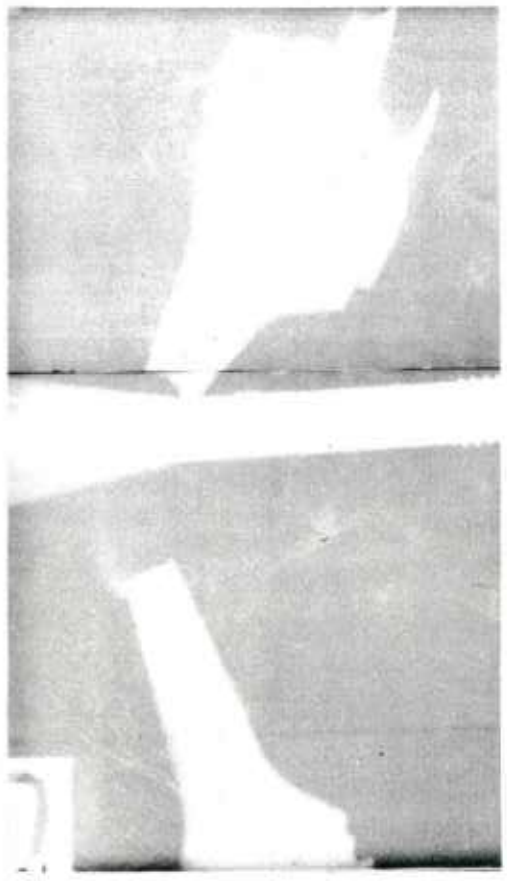

STANDARD SABOT COMPONENT

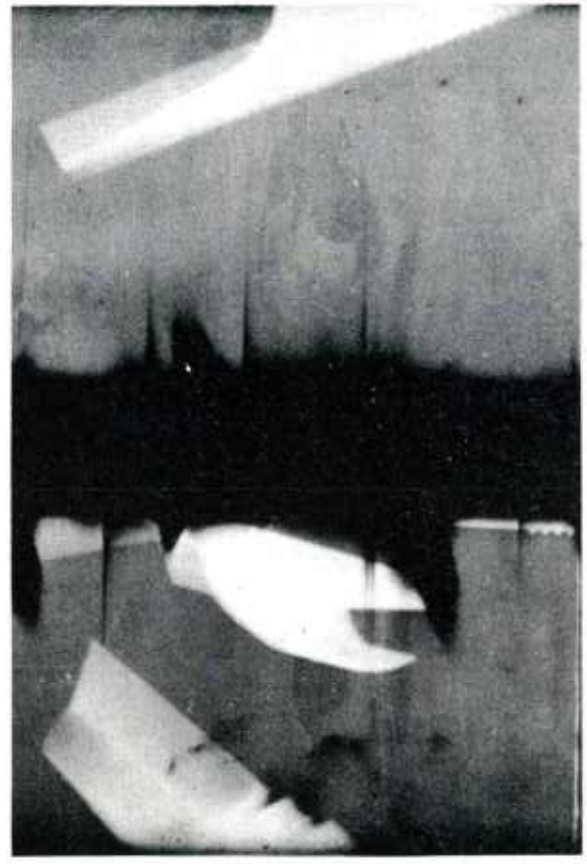

FINNED SABOT COMPONENT

FIG.(19) FLASH RADIOGRAPHS OF TWO SABOT COMPONENTS TAKEN 9.0 METERS FROM MUZZLE OF A CANNON.

REFERENCES

1. H. Conn, "The Influence of Sabot Separation on the Yawing Motion of a Cone," Defense Research Establishment, Valcartier, Canada, TN 1849/70, June 1970.

2. W. D. Glauz, "Estimation of Forces on a Flechette Resulting from a Shock Wave," Midwest Research Institute, Kansas City, MO, R3451-E, May 1971.

3. E. M. Schmidt and D. D. Shear, "Aerodynamic Interference During Sabot Discard," AIAA JSR, Vol. 15, No. 3, May-June 1978, pp 162-167.

4. E. M. Schmidt, "Disturbances to the Launch of Fin-Stabilized Projectiles," AIAA JSR, Vol. 19, No. 1, January-February 1982, pp 30-35.

5. D. Siegelman and P. Crimi, "Projectile/Sabot Discard Aerodynamics," Ballistic Research Laboratory, APG, MD, CR-00410, December 1979 (AD 080538).

6. D. Siegelman, P. Crimi, and E. M. Schmidt, "Projectile/Sabot Discard Aerodynamics," AIAA Paper No. 80-1588, August 1980.

7. D. Siegelman, J. Wang, and E. M. Schmidt, "Sabot Design Optimization," AIAA JSR, Vol. 19, No. 3, May-June 1982, pp 197-198.

8. E. M. Schmidt, "Wind-Tunnel Measurements of Sabot-Discard Aerodynamics," AIAA JSR, Vol. 18, No. 3, May-June 1981, pp 235-240.

9. G. Glotz, "Investigation of the Stability of Flow during the Sabot Discard Process," Proceedings of the 6th International Symposium on Ballistics, American Defense Preparedness Association, Arlington, VA, October 1981.

10. G. Moretti and M. Abbett, "A Time-Dependent Computational Method for Blunt Body Flows," AIAA J, Vol. 4, No. 12, Dec 1966, pp 2136-2141.

11. P. Plostins and S. G. Rubin, "The Axisymmetric Stagnation Region Full Shock Layer for Large Rates of Injection," Journal of Numerical Heat Transfer, Vol. 4, 1981, pp 358-375.

12. J. Sims, "Supersonic Flow around Right Circular Cones," Army Ballistic Missile Agency, Redstone Arsenal, AL, DA-TR-11-60, Mar 1960.

LIST OF SYMBOLS

d ..... Projectile Diameter
h ..... defined in equation (1b-c)
m ..... Mass Flux
M ..... Mach Number
p,P ... Pressure
Re .... Reynolds Number
t ..... Time
T ..... Temperature
u ..... Tangential Velocity
v ..... Normal Velocity
V ..... Freestream Velocity
x ..... Tangential Coor. or Projectile Axis
Δx .... Sabot Forward Movement
y ..... Normal Coordinate
Δy .... Sabot Lateral Movement

GREEK SYMBOLS

α ..... Angle of Attack
β ..... Non-Dim. Normal Coordinate
Δ ..... Standoff Distance
ϕ ..... Transverse Coordinate
ρ ..... Density

SUBSCRIPTS

ff .... Front Face
s ..... Stagnation or Shock Value
∞ ..... Freestream Conditions

SUPERSCRIPTS

$\bar{}$ ..... Non-Dim. with Freestream Values
$\hat{}$ ..... Non-Dim. with Shock Values

DISTRIBUTION LIST

No. of Copies	Organization
12	Administrator Defense Technical Info Center ATTN: DTIC-DDA Cameron Station Alexandria, VA 22314
1	Commander US Army Materiel Development and Readiness Command ATTN: DRCDMD-ST 5001 Eisenhower Avenue Alexandria, VA 22333
2	Commander US Army Materiel Development and Readiness Command ATTN: DRCDL DRCDE-R, Mr. Lockert 5001 Eisenhower Avenue Alexandria, VA 22333
4	Commander US Army Aviation Research and Development Command ATTN: Tech Dir (Mr. R. Lewis) DRDAV-E DRCPM-AAH (Mr. Corgiatt) Product Manager, AH-1 4300 Goodfellow Boulevard St. Louis, MO 63120
1	Director US Army Air Mobility Research and Development Laboratory Ames Research Center Moffett Field, CA 94035
1	Commander US Army Electronics Research and Development Command Technical Support Activity ATTN: DELSD-L Fort Monmouth, NJ 07703
1	President US Army Aviation Test Board ATTN: ATZQ-OP-AA Ft. Rucker, AL 36362
1	Commander US Army Medical Research and Development Command ATTN: SGRD-ZBM-C/LTC Lamothe Ft. Detrick, MD 21701
1	Commander US Army Communications Rsch and Development Command ATTN: DRSEL-ATDD Fort Monmouth, NJ 07703
4	Commander US Army Missile Command ATTN: DRSMI-R DRSMI-YDL DRSMI-TLH DRSMI-RDK Redstone Arsenal, AL 35898
1	Commander US Army Tank Automotive Command ATTN: DRSTA-TSL Warren, MI 48090
1	Commander US Army Armament Materiel Readiness Command ATTN: DRSAR-LEP-L Rock Island, IL 61299

DISTRIBUTION LIST

No. of Copies	Organization
9	Commander US Army Armament Research and Development Command ATTN: DRDAR-TSS DRDAR-TDS, Mr. Lindner DRDAR-LC-F, Mr. Loeb DRDAR-SCA, Mr. N. Ford DRDAR-LCW, Mr. M. Salsbury DRDAR-LCW, Mr. R. Wrenn DACPM-CAWS, Mr. Barth DRDAR-SEM, W. Bielauskas Dover, NJ 07801
1	ODCSI, USAREUR & 7A ATTN: AEAGB-PDN(S&E) APO, NY 09403
1	Director Division of Medicine WRAIR/WRAMC ATTN: SGRD-UWH-D/MAJ Jaeger Washington, DC 20012
6	Commander US Army Armament Research and Development Command ATTN: DRDAR-LCV, Mr. Reisman DRDAR-SCA, Mr. Kahn DRDAR-LC, Dr. Frasier DRDAR-SCW, Mr. Townsend DRDAR-TDC, Dr. Gyorog DRDAR-SG, Dr. T. Hung Dover, NJ 07801
4	Director US Army ARRADCOM Benet Weapons Laboratory ATTN: DRDAR-LCB-TL CPT R. Dillon Dr. G. Carofano Dr. C. Andrade Watervliet, NY 12189

No. of Copies	Organization
1	Commander US Army Jefferson Proving Ground ATTN: STEJP-TD-D Madison, IN 47251
1	Commander US Army Materials and Mechanics Research Center ATTN: DRXMR-ATL Watertown, MA 02172
1	Commander US Army Natick Research and Development Command ATTN: DRDNA-DT, Dr. D. Sieling Natick,MA 01762
1	Commander US Army Aeromedical Research Laboratory ATTN: SGRD-UAH-AS, Dr. Patterson P.O. Box 577 Ft. Rucker, AL 36362
2	Director US Army TRADOC Systems Analysis Activity ATTN: ATAA-S ATAA-SL White Sands Missile Range NM 88002
2	Commandant US Army Infantry School ATTN: ATSH-CD-CSO-OR FT Benning, GA 31905
1	Commander US Army Research Office ATTN: CRD-AA-EH P.O. Box 12211 Research Triangle Park NC 27709

DISTRIBUTION LIST

No. of Copies	Organization
1	Commander US Army Ballistic Missile Defense Systems Command P.O. Box 1500 Huntsville, AL 35807
3	Commander Naval Air Systems Command ATTN: AIR-604 Washington, DC 20360
3	Commander Naval Sea Systems Command ATTN: ORD-9132 Washington, DC 20362
2	Commander David W. Taylor Naval Ship Research & Development Center ATTN: Lib Div, Code 522 Aerodynamic Lab Bethesda, MD 20084
3	Commander Naval Surface Weapons Center ATTN: 6X Mr. F. H. Maille Dr. J. Yagla Dr. G. Moore Dahlgren, VA 22448
1	Commander Naval Surface Weapons Center ATTN: Code 730, Tech Lib Silver Spring, MD 20910
1	Commander Naval Weapons Center ATTN: Code 3431, Tech Lib China Lake, CA 93555
1	Commander Naval Weapons Center ATTN: Tech Info Div Washington, DC 20375
1	Commander Naval Ordnance Station ATTN: Code FS13A, P. Sewell Indian Head, MD 20640
1	AFRPL/LKCB Edwards AFB, CA 93523
2	AFATL (DLDL, Dr. D. C. Daniels) Tech Lib) Eglin AFB, FL 32542
1	AFWL/SUL Kirtland AFB, NM 87115
1	AFAL/WRW Wright-Patterson AFB, OH 45433
1	Director National Aeronautics and Space Administration George C. Marshall Space Flight Center ATTN: MS-I, Lib Huntsville, AL 38512
1	Director Jet Propulsion Laboratory ATTN: Tech Lib 2800 Oak Grove Drive Pasadena, CA 91103

DISTRIBUTION LIST

No. of Copies	Organization
1	Director NASA Scientific & Technical Information Facility ATTN: SAK/DL P. O. Box 8757 Baltimore/Washington International Airport, MD 21240
1	AAI Corporation ATTN: Dr. T. Stastny Cockeysville, MD 21030
1	Advanced Technology Labs ATTN: Mr. J. Erdos Merrick & Stewart Avenues Westbury, NY 11590
1	Aerospace Corporation ATTN: Dr. G. Widhopf P. O. Box 92957 Los Angeles, CA 90009
1	ARTEC Associates, Inc. ATTN: Dr. S. Gill 26046 Eden Landing Road Hayward, CA 94545
1	AVCO Systems Division ATTN: Dr. D. Siegelman 201 Lowell Street Wilmington, MA 01887
1	Director Forrestall Research Center Princeton University Princeton, NJ 08540
1	Battelle Memorial Institute ATTN: J. E. Backofen, Jr. 505 King Avenue Columbus, OH 43201
1	Technical Director Colt Firearms Corporation 150 Huyshope Avenue Hartford, CT 14061
2	ARO, Inc Von Karman Gasdynamics Facility ATTN: Dr. J. Lewis Mr. W. D. Williams Arnold AFS, TN 37389
1	General Electric Corporation Armaments Division ATTN: Mr. R. Whyte Lakeside Avenue Burlington, VT 05401
1	Honeywell, Inc. ATTN: Mail Station MN 112190 (G. Stilley) 600 Second Street, North Hopkins, MN 55343
1	Southwest Research Institute ATTN: Mr. P. Westine 8500 Culebra Road San Antonio, TX 78228

DISTRIBUTION LIST

No. of Copies	Organization
4	Hughes Helicopter Company Bldg. 2, MST22B ATTN: Mr. R. Forker Mr. M. Kane Mr. R. Flood Mr. L. Johnson Centinella & Teal Streets Culver City, CA 90230
1	Martin Marietta Aerospace ATTN: Mr. A. J. Culotta P. O. Box 5387 Orlando, FL 32805
1	Olin Corporation Winchester-Western Division New Haven, CT 06504
1	Sandia Laboratories ATTN: Aerodynamics Dept Org 5620, R. Maydew Albuquerque, NM 87115
1	Guggenheim Aeronautical Lab California Institute of Tech ATTN: Tech Lib Pasadena, CA 91104
1	Franklin Institute ATTN: Tech Lib 20th & Parkway Philadelphia, PA 19103
1	Director Applied Physics Laboratory The Johns Hopkins University Johns Hopkins Road Laurel, MD 20707
1	Massachusetts Institute of Technology Dept of Aeronautics and Astronautics ATTN: Tech Lib 77 Massachusetts Avenue Cambridge, MA 02139
1	Ohio State University Dept of Aeronautics and Astronautical Engineering ATTN: Tech Lib Columbus, OH 43210
2	Polytechnic Institute of New York Graduate Center ATTN: Tech Lib Prof. R. J. Cresci Route 110 Farmingdale, NY 11735
1	Kaman Tempo ATTN: Mr. J. Hindes 816 State Street P.O. Drawer QQ Santa Barbara, CA 93102

DISTRIBUTION LIST

Aberdeen Proving Ground

Dir, USAMSAA
ATTN: DRXSY-D
DRXSY-MP, H. Cohen

Cdr, USATECOM
ATTN: DRSTE-TO-F

Cdr, USACSL, Bldg. E3516, EA
ATTN: DRDAR-CLB-PA
DRDAR-CLN
DRDAR-CLJ-L

Dir, USAHEL
ATTN: Dr. Weisz

USER EVALUATION OF REPORT

Please take a few minutes to answer the questions below; tear out this sheet, fold as indicated, staple or tape closed, and place in the mail. Your comments will provide us with information for improving future reports.

1. BRL Report Number _____

2. Does this report satisfy a need? (Comment on purpose, related project, or other area of interest for which report will be used.)

_____

_____

_____

3. How, specifically, is the report being used? (Information source, design data or procedure, management procedure, source of ideas, etc.) _____

_____

_____

4. Has the information in this report led to any quantitative savings as far as man-hours/contract dollars saved, operating costs avoided, efficiencies achieved, etc.? If so, please elaborate.

_____

_____

5. General Comments (Indicate what you think should be changed to make this report and future reports of this type more responsive to your needs, more usable, improve readability, etc.) _____

_____

_____

_____

6. If you would like to be contacted by the personnel who prepared this report to raise specific questions or discuss the topic, please fill in the following information.

Name: _____

Telephone Number: _____

Organization Address: _____

_____

_____